Food Research International 172 (2023) 113080

Contents lists available at ScienceDirect

Food Research International

journal homepage: www.elsevier.com/locate/foodres

Engineering multicomponent tissue by spontaneous adhesion of myogenic and adipogenic microtissues cultured with customized scaffolds

N. Stephanie Kawecki [a,b], Sam C.P. Norris [a], Yixuan Xu [c], Yifan Wu [b], Ashton R. Davis [a,d], Ester Fridman [a], Kathleen K. Chen [a,d], Rachelle H. Crosbie [a,e,i], Andrea J. Garmyn [f], Song Li [b,h,i,j], Thomas G. Mason [d,g,j], Amy C. Rowat [a,b,h,i,j,*]

[a] Department of Integrative Biology and Physiology, University of California, Los Angeles, Los Angeles, CA 90095, USA
[b] Department of Bioengineering, University of California, Los Angeles, Los Angeles, CA 90095, USA
[c] Department of Materials Science and Engineering, University of California, Los Angeles, Los Angeles, CA 90095, USA
[d] Department of Chemistry and Biochemistry, University of California, Los Angeles, Los Angeles, CA 90095, USA
[e] Department of Neurology, David Geffen School of Medicine, University of California LA, USA
[f] Department of Food Science and Human Nutrition, Michigan State University, East Lansing, MI 48824, USA
[g] Department of Physics and Astronomy, University of California, Los Angeles, Los Angeles, CA 90095, USA
[h] Jonsson Comprehensive Cancer Center, University of California, Los Angeles, Los Angeles, CA 90095, USA
[i] Broad Stem Cell Center, University of California, Los Angeles, Los Angeles, CA 90095, USA
[j] California NanoSystems Institute, University of California, Los Angeles, Los Angeles, CA 90095, USA

ARTICLE INFO

Keywords:
Cellular agriculture
Cultured meat
Tissue engineering
Tissue-engineered skeletal muscle
Tissue-engineered adipose tissue
Scaffold

ABSTRACT

The integration of intramuscular fat—or marbling—into cultured meat will be critical for meat texture, mouthfeel, flavor, and thus consumer appeal. However, culturing muscle tissue with marbling is challenging since myocytes and adipocytes have different media and scaffold requirements for optimal growth and differentiation. Here, we present an approach to engineer multicomponent tissue using myogenic and adipogenic microtissues. The key innovation in our approach is the engineering of myogenic and adipogenic microtissues using scaffolds with customized physical properties; we use these microtissues as building blocks that spontaneously adhere to produce multicomponent tissue, or marbled cultured meat. Myocytes are grown and differentiated on gelatin nanofiber scaffolds with aligned topology that mimic the aligned structure of skeletal muscle and promotes the formation of myotubes in both primary rabbit skeletal muscle and murine C2C12 cells. Preadipocytes are cultured and differentiated on edible gelatin microbead scaffolds, which are customized to have a physiologically-relevant stiffness, and promote lipid accumulation in both primary rabbit and murine 3T3-L1 pre-adipocytes. After harvesting and stacking the individual myogenic and adipogenic microtissues, we find that the resultant multicomponent tissues adhere into intact structures within 6–12 h in culture. The resultant multicomponent 3D tissue constructs show behavior of a solid material with a Young's modulus of $\sim 2 \pm 0.4$ kPa and an ultimate tensile strength of $\sim 23 \pm 7$ kPa without the use of additional crosslinkers. Using this approach, we generate marbled cultured meat with $\sim$ mm to $\sim$ cm thickness, which has a protein content of $\sim 4 \pm 2$ g/100 g that is comparable to a conventionally produced Wagyu steak with a protein content of $\sim 9 \pm 4$ g/100 g. We show the translatability of this layer-by-layer assembly approach for microtissues across primary rabbit cells, murine cell lines, as well as for gelatin and plant-based scaffolds, which demonstrates a strategy to generate edible marbled meats derived from different species and scaffold materials.

1. Introduction

Culturing meat ex vivo has potential to complement existing methods for animal protein production to increase the sustainability and resiliency of our food system (Gherman & Bălan, 2022). The concept of culturing cells as a complement for protein production was envisioned by Winston Churchill in 1931 (Churchill, 2016); nearly a century later, a cultured meat burger became a reality in a pioneering demonstration led

* Corresponding author at: Department of Integrative Biology and Physiology, University of California, Los Angeles, Los Angeles, CA 90095, USA.
E-mail address: rowat@ucla.edu (A.C. Rowat).

https://doi.org/10.1016/j.foodres.2023.113080
Received 6 December 2022; Received in revised form 29 May 2023; Accepted 30 May 2023
Available online 29 June 2023

by Mark Post (Fountain, 2013). More recent advances in cellular agriculture demonstrate the feasibility of engineering ground meat mimics, such as cultured beef burgers (Norris et al., 2022) and meatballs (Liu et al., 2022), as well as structured, 3D muscle tissues as meat analogs (Furuhashi et al., 2021; MacQueen et al., 2019; Xiang, Yuen Jr, et al., 2022). Taste, however, remains a major consumer concern (Tomiyama et al., 2020); thus strategies to enhance the palatability—or deliciousness—of cultured meat are a top priority. A major contributor to meat flavor, texture, and nutrient properties is intramuscular fat or marbling (Hocquette et al., 2010; Nishimura et al., 1999; Post et al., 2020; Savell et al., 1987; Tuma et al., 1962; Wood et al., 1999). The amount of intramuscular fat is positively correlated with desired meat flavor, juiciness, and tenderness, and therefore consumer appeal (Noidad et al., 2019; O'Quinn et al., 2018). To make cultured meat products that consumers desire—such as a USDA Prime or Wagyu steak (O'Quinn et al., 2018)—it will be critical to develop strategies to engineer muscle tissue with spatially organized intramuscular fat. Furthermore, it will be important to make delicious and nutritious cultured meat accessible, which necessitates that marbling in cultured meats is generated using a scalable process that is compatible with food production.

One approach to generate cultured meat that contains fat tissue is to co-culture myogenic and adipogenic cells. Multicomponent cultured meat has been successfully demonstrated by co-culture of different cell types including bovine skeletal muscle cells, smooth muscle cells, and endothelial cells on a porous scaffold (Ben-Arye et al., 2020). However, a randomly mixed co-culture approach results in a homogeneous distribution of cells throughout the tissue construct and does not achieve the spatial patterning required for marbling. Furthermore, different cell types typically have different media requirements for optimal growth (Ricotti et al., 2012; Zebisch et al., 2012), which challenges co-culturing in a bioreactor system that is desired for scale up (Allan et al., 2019). To achieve cultured meat with marbling, scaffolds provide a strategy to introduce structure into engineered tissue constructs from the level of individual cells to supracellular features (Kim et al., 2017; MacQueen et al., 2019; Norris et al., 2022). For example, edible microcarrier scaffolds with grooved topology that mimic skeletal muscle can promote the alignment of myogenic cells (Norris et al., 2022). Scaffolds with aligned topology can also improve the differentiation efficiency of myogenic cells into multinucleated myotubes, which are precursors of muscle fibers (Furuhashi et al., 2021; Huang et al., 2006; MacQueen et al., 2019; Qazi et al., 2015; Yeo & Kim, 2019). Scaffold-cell constructs can additionally support the patterning of fat features in cultured muscle using 3D printing (Kang et al., 2021) or by stacking scaffold-cell sheets (Li et al., 2022). Importantly, scaffolds can also regulate cellular behaviors that are critical contributors to the growth of cultured meat. For example, adipogenic murine 3T3-L1 cells show increased lipid accumulation when cultured within a more compliant alginate scaffold with a Young's modulus of ~ 2 kPa compared to stiffer, ~12 kPa scaffolds (Chandler et al., 2011); while substrates with ~ 12–14 kPa stiffness have been shown to increase the differentiation efficiency of muscle cells (Engler et al., 2004). Thus, strategies to engineer customized scaffolds that support the growth of individual types of microtissues—which are building blocks for multicomponent tissue—could ultimately enable the efficient production of marbled cultured meat that consumers desire.

Here we present a modular strategy to engineer marbled cultured meat. The key innovation in our approach is the generation of ~ mm to ~ cm scale multicomponent tissue constructs using myogenic and adipogenic microtissues as spontaneously adhering building blocks; microtissue growth is enabled by scaffolds with physical properties that are customized for both myocytes and adipocytes. We proliferate and differentiate myocytes on nanofiber scaffolds with aligned topology, which mimics the aligned structure of skeletal muscle tissue (Schiaffino & Reggiani, 2011). In parallel, pre-adipocytes are proliferated and differentiated on microbead scaffolds with a Young's modulus of ~ 4 kPa, which mimics the stiffness of adipose tissue (Comley & Fleck, 2010). We show how these customized scaffolds can support the growth of both primary rabbit cells as well as murine cell lines. Moreover, the modular approach using customized scaffolds has scalable potential as it relies on the spontaneous adhesion of cells and scaffolds to form myogenic and adipogenic microtissues as well as 3D multicomponent tissues, or marbled cultured meat.

2. Methods

2.1. Nanofiber scaffold fabrication

Nanofiber scaffolds are fabricated using a custom-built electrospinner. The electrospinner is assembled using a 30 kV power supply (Gamma High Voltage), syringe pump (Harvard Apparatus), and custom-built rotating aluminum collection cylinder (18 cm length, 6 cm diameter) mounted to a high-speed AC motor (Baldor). The number of cylinder rotations per minute (RPM) is adjusted using an AC to DC converter with speed control (Variac). The entire electrospinning device is enclosed in an environmentally-controlled chamber to maintain an ambient temperature of 37 °C using a space heater (Honeywell). To fabricate nanofibers, we use gelatin type B derived from bovine skin (Sigma) and gelatin dissolved in MilliQ water at a concentration of 15 w/v% in a 55 °C water bath. The prepolymer solution is loaded into a 3 mL syringe with Luer Lock tip attached to an 18-gauge flat needle. To generate sheets of gelatin fibers, we electrospin 300 μL of gelatin solution at 12 kV with a flowrate of 5 μL/min, and a distance of 7 cm from the syringe tip to the collection cylinder. To obtain aligned nanofibers, we spin the collection cylinder at ~ 10,000 RPM; unaligned nanofibers are generated by spinning at ~ 1,000 RPM. To ensure mechanical stability of nanofiber sheets during cell culture, we chemically crosslink the nanofibers after cooling to room temperature (RT) by submerging them in a solution of 38 mg/mL 1-ethyl-3-(3-dimethylaminopropyl) carbodiimide hydrochloride (EDC-HCl, Chem IMPEX) in 100 % ethanol for 18 h. Crosslinked nanofibers are rinsed 3 times with 1 × Phosphate Buffer Solution (PBS, Corning), and either mounted on poly-l-lysine slides for 2D cultures or mounted on tissue culture plates using custom-made rubber inserts for 3D cultures. Prior to cell seeding, all scaffolds are sterilized with 70 % ethanol for 15 min, and subsequently rinsed 3 times with sterile 1 × PBS.

2.2. Microbead scaffold fabrication

Gelatin microbeads are fabricated using the droplets of water-in-oil emulsions as templates, as described previously by our lab and others (Leal-Calderon et al., 2007; Norris et al., 2022; Nyberg et al., 2017; Poncelet et al., 1992). In brief, a prepolymer solution with 4 % gelatin derived from bovine skin (Sigma) and 4 % microbial transglutaminase (MTG) powder (Activia TI, Ajinomoto) is prepared in MilliQ water; 1 mL of the prepolymer solution is then immediately pipetted into a beaker of 9 g light mineral oil (Fisher) containing 1 w/w% of Span 80 (TCI America). The emulsion is placed in a bath of 55 °C water; over 24 h with continuous stirring the bath is allowed to reach RT. To retrieve the microbeads from the emulsion, we remove the oil phase by washing 3 times with hexane (Sigma) and centrifuge at 1000 RCF for 5 min, followed by resuspension in 20 mL of 1× PBS with 0.1 % Tween 80 (Fisher). Microbeads are then placed in a 75 °C water bath for 10 min to evaporate remaining hexane and deactivate microbial transglutaminase. The microbead suspensions are again washed 3 times with 1× PBS with 0.1 % Tween 80 and incubated overnight to allow microbeads to fully swell prior to filtering beads. To obtain microbeads that range in diameter from 60 to 100 μm—which are within the size range of commercially-available microbeads (Chen et al., 2011)—microbeads are size-filtered by passing sequentially through a 100 μm filter followed by a 60 μm filter (PluriSelect USA). The beads are collected from the top surface of the 60 μm filter and stored in 1× PBS with 0.1 % Tween 80 at 4 °C until use. To control the cell seeding density, we quantify the surface area per microbead using light microscopy and quantitative image

analysis as previously described (Norris et al., 2022). To prepare microbeads for cell culture, we sterilize microbeads in 70 % ethanol for 15 min, wash 3 times in 1 × PBS, incubate overnight in 1 × PBS with 0.1 % Tween 80 to ensure microbeads are fully swollen, and then resuspend after centrifugation (1000 RCF, 5 min) in cell culture medium. Following a previously developed protocol (Norris et al., 2022), we adjust the concentration of microbeads in solution to 8.8 cm^2/mL.

2.3. Plant-based scaffolds

Zein microfiber scaffolds are obtained from Matrix F.T. Within a sterile culture hood, scaffolds are cut into 0.5 × 0.5 cm pieces, washed 3 times with sterile water, and washed 1 time with cell culture medium. Soy microcarriers (Matrix F.T.) are rinsed 3 times with sterile water and resuspended in cell culture medium and loaded into wells at a concentration of 5 mg/mL.

2.4. Mechanical characterization of scaffolds

To determine scaffold stiffness, we measure the Young's modulus of the nanofiber sheets and microbeads in 1× PBS with 0.1 % Tween 80 using a JPK Nanowizard 4a BioScience AFM in force spectroscopy mode. The scaffolds are adhered to a poly-L-lysine coated slide (Epredia) and indented with a SAA-SPH-5UM probe (Bruker) with a 10 μm diameter spherical tip. The spring constants of the probes are individually calibrated by the manufacturer. Single indentations are performed with a total force of 4.0 nN. Since an oblique contact between the spherical AFM probe and the scaffold surface can result in inaccurate force curve fitting, indentations are performed on the top surface of the scaffold. Young's modulus values are determined by averaging over 5 unique indentations each scaffold. All force curve analysis is performed using the JPK Data Processing software. Young's modulus values are calculated by using a Hertz/Sneddon spherical fit with a Poisson's ratio of $\nu = 0.5$ (Mott & Roland, 2009). For plant-based zein microfiber scaffolds and soy microcarriers, we measure the Young's Modulus by microindentation (Pavone, Optics11) using a probe with 10 μm diameter and 0.51 N stiffness. Force curve analysis is performed using the Optics 11 Data Viewer. Young's modulus values are calculated using a Hertzian contact fit assuming a Poisson's ratio of $\nu = 0.5$.

2.5. Cell culture

Mouse myogenic cells (C2C12, ATCC CRL-1772) are cultured in Dulbecco's Modified Eagle's Medium (DMEM) (Gibco, 4.5 g/L glucose, l-glutamine, 110 mg/L sodium pyruvate) with 10 % fetal bovine serum (FBS, GemCell™, Gemini). To induce myogenic differentiation and myotube formation, cells are cultured in differentiation medium consisting of DMEM with 2 % donor horse serum (HS, Gemini GemCell™). Mouse pre-adipocytes (3T3-L1, ATCC CL-173), which are commonly used as a model for adipogenesis (Chandler et al., 2011; Fischbach et al., 2004; Frye & Patrick, 2006), are cultured in DMEM with 10 % super calf serum (SCS, GemCell™, Gemini). To induce differentiation into adipocytes, 3T3-L1 cells are cultured in DMEM with 10 % FBS, 0.25 μM dexamethasone (Sigma), 10 μg/mL bovine insulin (Sigma), 0.5 mM 3-isobutyl-1-methylxanthine (IBMX, Sigma), and 0.2 mM ascorbic acid 2-phosphate (Sigma). We culture C2C12 and 3T3-L1 cells for ≤10 passages and confirm their identity using Short Tandem Repeat (STR) profiling. Primary rabbit myoblasts (RbSkMC, Cell Applications, Rb150-05) are cultured in RbSkMC growth medium (Cell Applications, Rb151-500) and differentiated into myotubes by culturing in RbSkMC differentiation medium (Cell Applications, Rb151D-250). Primary rabbit pre-adipocytes from subcutaneous fat (RbPreAd, Cloud Clone, CSI032RB01) are cultured in DMEM with 20 % fetal bovine serum (FBS, GemCell™, Gemini). To induce differentiation into adipocytes, rabbit pre-adipocytes are cultured in DMEM with 10 % FBS, 0.25 μM dexamethasone (Sigma), 10 μg/mL bovine insulin (Sigma), 0.5 mM 3-isobutyl-1-methylxanthine (IBMX, Sigma) and 0.2 mM ascorbic acid 2-phosphate (Sigma). Primary rabbit cells are cultured for < 5 passages. All cells are cultured with 1× antibiotic–antimycotic (Gibco) at 37 °C and 5 % CO_2.

2.6. Multicomponent tissue production

To show proof-of-concept multicomponent tissue, we generate myogenic microtissue consisting of differentiated muscle cells on nanofibers and adipogenic microtissue consisting of adipocytes on microbeads. To produce myogenic microtissue, precursor muscle cells are seeded at a density of 3×10^3 cells/cm^2 on gelatin nanofiber and zein microfiber scaffolds. When cells reach 100 % confluency, myocytes are differentiated for 7 days by replacing the media with differentiation induction medium. To generate adipogenic microtissue, adipocytes are cultured on gelatin microbeads or soy microcarriers in non-tissue culture wells. To reduce cell adhesion, plates are treated prior to use with sterile 0.2 % Pluronic solution for 10 min, followed by aspirating, air drying, and washing 3 times with 1× PBS. Pre-adipocytes are seeded at 100,000 cells per 8.8 cm^2 of gelatin microbeads in 1 mL of cell culture media in the pre-coated tissue culture plates, proliferated until 100 % confluency, and differentiated for 7 days under static conditions. Pre-adipocytes are seeded at 5×10^5 cells/mL onto soy microcarriers (1 mL of 5 mg/mL) loaded into wells as per the manufacturer's instructions. To generate multicomponent tissue constructs, we manually stack myogenic and adipogenic microtissues to create a layered tissue construct. Multicomponent tissues are incubated for up to 18 h in culture (37 °C, 5 % CO_2) in DMEM with 10 % fetal bovine serum (FBS, GemCell™, Gemini) and 1× antibiotic–antimycotic (Gibco) prior to harvesting. For multicomponent tissue (MT), samples are analyzed immediately after removal from culture for imaging and rheology analyses. For our rheology analysis, we refer to these samples as direct-from-culture MT. We also test samples with reduced water content in rheology, tensile, protein content, and cooking loss analyses by removing MT samples from culture and placing on filter paper (Whatman) for 24 h at 4 °C.

2.7. Relative adhesion assay

To investigate the spontaneous adhesion of stacked myogenic and adipogenic microtissues across cell and scaffold types, we developed an adhesion assay to quantify how intact a stack of microtissues remains after mechanical perturbation. To generate a stack of microtissues, we place differentiated adipocytes cultured on gelatin microcarriers onto a layer of differentiated myotubes on aligned gelatin nanofiber scaffolds. We also investigate the adhesion of myogenic and adipogenic microtissues cultured with plant-based scaffolds by placing differentiated primary rabbit pre-adipocytes on soy microcarriers onto a layer of differentiated rabbit myotubes on aligned zein microfiber scaffolds. As a control, we test scaffolds without cells, where soy microcarriers are placed on zein microfiber scaffolds. Each stack of myogenic and adipogenic microtissues or scaffold-only control is placed in the well of a 48-well plate together with 200 μL of 1 × PBS. To test how intact the stack is after mechanical perturbation, we subject the samples to rigorous nutation at 100 RPM for 2 min at 0, 6, 12, and 18 h post stacking. By acquiring brightfield images of each stack before and after nutating, we determine the projected surface area (*SA*) of the microtissues/scaffolds before and after nutation using quantitative image analysis. When microtissues/scaffolds are adhered to each other, the stack remains intact and there is no observable change in the projected surface area of the microtissues/scaffolds after nutating. By contrast when samples are not adhered, the rigorous nutation displaces microtissues/scaffolds and they are released into the culture dish resulting in an increase in the projected surface area. We determine the relative adhesion index by $[100 - (SA_{before} - SA_{after})]$ and assess the timescale of adhesion by quantifying at 0, 6, 12, and 18 h timepoints.

2.8. Confocal imaging and quantitative image analysis

To visualize cellular and scaffold components of the 3D multicomponent tissues, gelatin microbeads are fluorescently labeled with BODIPY (BDY 650-X, SE, Tocris Bioscience™) prior to cell culture. In brief, beads are centrifuged and resuspended in 1× PBS with 1 μg/mL BODIPY for 1 h. Subsequently, beads are washed 3 times with 1× PBS prior to ethanol sterilization as described in section 2.2. To visualize multicomponent tissue cross-sections, samples are flash frozen using standard methods (Kumar et al., 2015). We cool 250 mL of methylbutane by submerging a beaker in liquid nitrogen for 30 min. Tissue samples are submerged in Optimal Cutting Temperature (OCT) compound and placed on a cryomold. Cryomolds with tissue samples are then submerged in chilled methylbutane for ~ 30 s and placed on dry ice in a fume hood to allow for evaporation of excess methylbutane. Samples are cryosectioned into 50 μm-thick slices and placed on a poly-l-lysine-coated slide using standard protocols. To prepare for immunostaining, samples are rinsed 3 times with 1× PBS and fixed with 4 % paraformaldehyde (PFA, Sigma) for 15 min at RT followed by cell permeabilization with 1× PBS with 0.1 % triton-X for 5 min at RT. To minimize non-specific binding, cultures are placed in 1× PBS with 1 % BSA (Fisher) and 0.1 % Tween 20 for 15 min at RT. To label myogenic microtissues, samples are immunostained to visualize myosin heavy chain (Myh4) (MF20, 1:200, eBioscienceTM, Invitrogen and Alexa-Fluor 594 goat anti-mouse, 1:500, Invitrogen) for 24 h; DNA is labeled using Hoechst 3334 (trihydrochloride trihydrate, 1:1000, Life Technologies) for 1 h. Adipogenic microtissues are labeled to visualize peroxisome proliferator-activated receptor gamma (PPARγ K.242.9, 1:100, Invitrogen, Alexa-Fluor 555 rabbit anti-goat, 1:500, Invitrogen) for 24 h, as well as neutral lipids (LipidTox, 1:200, Invitrogen, Nile Red, 1:3000, Acros Oranics) and DNA (Hoechst 33342, 1:1000, trihydrochloride trihydrate, Life Technologies) for 1 h. Multicomponent tissues are incubated with antibodies for both myogenic and adipogenic components: primary antibodies (MF20, 1:200, eBioscienceTM, Invitrogen, PPARγ K.242.9, 1:100, Invitrogen) are incubated for 24 h and washed 3 times with 1× PBS. Secondary antibodies and stains are subsequently added and incubated for 4 h (Alexa-Fluor 594 goat anti-mouse, 1:500, Invitrogen; Alexa-Fluor 555 rabbit anti-goat, 1:500, Invitrogen; LipidTox, 1:200, Invitrogen, Nile Red, 1: 3000, Acros Oranics; Hoechst 33342, 1:1000, trihydrochloride trihydrate, Life Technologies). To compare multicomponent tissue with conventionally produced Wagyu steak (First Light), we visualize proteins in 50 μm-thick cryosections of Wagyu steak with fluorescein isothiocyanate (FITC, 1:1000, Thermofisher, 1 h incubation) and lipids using Nile Red (Nile Red, 1: 3000, Acros Oranics, 1 h incubation). Labeled samples are washed 3 times with 1× PBS, mounted using Fluoromount-G (Invitrogen), and imaged using a laser scanning confocal microscope (Zeiss LSM880) equipped with a 10× /0.45NA or 20× /0.8NA objective and using a pinhole of 1 AU. All widefield images are acquired with a Zeiss Observer Z1 using a 5× /0.13NA, 10× /0.31NA, or 20× /0.5 NA objective. Images are processed with Zen (Zeiss), Fiji, and Imaris (Bitplane) software. To quantify the extent of muscle cell differentiation, we compare the myogenic index by measuring the number of nuclei localized within a myotube in Myh4-positive cells relative to the total number of nuclei in the field of view (ImageJ) as shown in Supplementary Fig. 1. To quantify lipid accumulation, we measure the total surface area of LipidTox in thresholded images (ImageJ). To determine the average lipid area per cell, we divide the total lipid area by the total number of nuclei, which we quantify using Hoechst.

2.9. Quantitative real-time polymerase chain reaction (qRT-PCR)

To measure the extent of differentiation of C2C12 skeletal muscle cells on nanofibers and 3T3-L1 pre-adipocytes on microbeads, we quantify levels of transcripts that are markers of myogenesis and adipogenesis using qRT-PCR. Briefly, we perform whole-cell RNA extraction using TRIzol® reagent (Invitrogen) according to the manufacturer's protocol. Total RNA is further purified using the PureLink™ RNA Mini Kit (Invitrogen). Reverse transcriptase is performed to obtain cDNA using the SuperScript™ IV First-Strand Synthesis System (Invitrogen). Quantitative PCR is performed using the QuantStudio™ 5 Real-Time PCR System (Applied Biosystems) and PowerUp™ SYBR™ Green Master Mix (Applied Biosystems) with the following gene-specific primers: *Gapdh* mRNA (forward: 5′- TGAACGGATTTGGCCGTATT −3′, reverse: 5′- CTGGAACATGTAGACCATGTAGTT −3′), *Myh4* mRNA (forward: 5′- TCTACACTTACTCAGGCCTCTT −3′, reverse: 5′- CTGGTAGGCGTTATCAGAGATG −3′), *Myog* mRNA (forward: 5′- CAGTACATTGAGCGCCTACA −3′, reverse: 5′- TGGGAGTTGCATTCACTGG −3′), *Mef2C* mRNA (forward: 5′- CTGGCAGCTCTACACCATTG −3′, reverse: 5′- AAGCCTTCTTCATCAATCCAAA −3′), *18 s* mRNA (forward: 5′- CTGAGAAACGGCTACCACATC −3′, reverse: 5′- GCCTCGAAAGAGTCCTGTATTG −3′), *PPARγ* mRNA (forward: 5′- GCTGCAGCGCTAAATTCTTC −3′, reverse: 5′- AAGGAATGCGAGTGGTCTTC −3′), and *C/EBPalpha* mRNA (forward: 5′- CGGGCAAAGCCAAGAAGT −3′, reverse: 5′- GCAGCGTGTCCAGTTCA −3′).

2.10. Rheological analysis

To quantify the mechanical properties of multicomponent tissues, we produce tissue constructs with a diameter of ~ 25 mm. To perform the rheological analysis, first, a strain-controlled shear rheometer (Rheometrics RFS-II) is calibrated, both in magnitude of the complex shear modulus and crossover frequency, using a polymeric viscoelastic reference standard. Following this calibration, each tissue sample, having a thickness of 1 mm, is loaded onto a 25-mm diameter stainless steel parallel plate. To set the gap, the upper plate is lowered until the measured normal force increases from zero to ≈ 4 %; the gap is set to match the sample thickness to ≈ 0.001 mm. Subsequently, a strain sweep at an angular frequency of $\omega = 1$ rad/s from strain $\gamma = 0.01$ to 2 is measured. The measured shear elastic modulus is fit to a functional form, $G'(\gamma) = G'_p / [(\gamma / \gamma_y)^k + 1]$, to obtain the linear plateau shear elastic modulus G'_p, given by the low-γ -plateau. Here γ_y is a yield strain associated with the knee in $G'(\gamma)$ and k is a power law exponent associated with the nonlinear response of $G'(\gamma)$ towards higher strain. For MT samples that are measured direct-from-culture, the same procedure is repeated; yet the strain sweep is measured from a lower limit of $\gamma = 1 \times 10^{-3}$, thereby ensuring that a set of low-γ measurements are well within the linear stress–strain regime. For Wagyu steak samples, the lower limit of the strain sweep measurement is further reduced to $\gamma = 5 \times 10^{-4}$. To evaluate the Young's modulus, E, of these samples, we calculate values using the equation, $E = 2(1 + \nu)\, G'_p$, where ν is the Poisson ratio. For multicomponent tissue samples, we assume a Poisson's ratio of 0.5 as determined for gelatin (van Otterloo & Cruden, 2016). For Wagyu steak samples, we assume a Poisson's ratio of 0.45 as determined for bovine skeletal muscle (Kim, Yoo, Shin, & Demer, 2013). Reported values of γ_y are approximate, since the parallel plate geometry does not have a uniform strain field within the region between the two plates occupied by the sample.

2.11. Tensile analysis

To determine the tensile strength of multicomponent tissues, we place strips of raw meat with length = 5 cm, diameter = 0.5 cm, and thickness = 0.2 – 0.4 cm for both multicomponent tissue and Wagyu samples into the wedge grips of a Chatillon TCD 225 series Force Measurement System (Tangent Labs). Samples are subject to uniaxial load at a strain rate of 30 mm/min. We record stress and strain at a sampling rate of 1 Hz until break. Stress and strain are calculated from the load/distance data and normalized to the cross-sectional area of each sample. Ultimate tensile strength is determined by the maximum stress at which the sample breaks.

2.12. Protein content analysis

To perform protein content analyses, we first determine the mass of multicomponent tissue and Wagyu steak samples. Subsequently, samples are washed 3 times with 1× PBS and submerged in RIPA Lysis Buffer (Sigma) with protease inhibitor and placed on ice for 30 min. Samples are centrifuged at 12,600 RCF at 4 °C for 15 min. Subsequently, the supernatant is collected and used to determine protein concentrations using the BSA Pierce™ BCA Protein Assay Kit (ThermoFisher). Protein concentrations are normalized per gram of sample.

2.13. Cooking analysis

To perform cooking loss analyses, we record the mass of the multicomponent tissue and Wagyu steak samples prior to placing on a clamshell grill (Yedi) preheated to 165 °C. The samples are cooked until the internal temperature—as measured by a thermocouple (Grainger) inserted into the innermost section of each sample—reaches 65 °C. After cooling to RT, we record the mass of the cooked tissue constructs, which enables us to determine the cooking loss, $CookingLoss = [(m_i - m_f)/m_i] \times 100$, where m_i is the initial mass of the tissue construct prior to cooking, and m_f is the final mass after cooking.

3. Results

To generate marbled cultured meat, we fabricate scaffolds with customized physical properties to support the growth and differentiation of myocytes and adipocytes. Culturing myocytes and adipocytes separately also enables us to use optimal growth medium for each cell type. We use the resultant myogenic and adipogenic microtissues as building blocks to generate larger tissue constructs with dimensions of ~ cm width and ~ mm thickness (Fig. 1).

3.1. Aligned nanofiber scaffolds to support myogenesis

To promote the efficient growth of myocytes and subsequent differentiation into myotubes, we fabricate scaffolds with aligned topology that have been shown to accelerate muscle cell growth and differentiation (Huang et al., 2006; Qazi et al., 2015; Yeo & Kim, 2019). We produce aligned scaffolds using electrospinning, which is already being scaled in pharmaceutical (Omer et al., 2021) and textile industries (Persano, Camposeo, Tekmen, & Pisignano, 2013). As proof-of-concept, we begin by using gelatin as a scaffold material.

To fabricate aligned nanofibers, we spin fibers onto a rotating cylinder spinning at ~ 10,000 RPM (Fig. 2); this results in a 12 × 15 cm fiber mat that can be released from the cylinder, cut into a desired scaffold size, and spread onto a surface. To quantify the alignment of fibers, we determine the orientation angle of individual fibers in the scaffold relative to each other from 0–180° using quantitative image analysis (Fig. 2A). Compared to unaligned fibers produced by spinning at a lower rotational speed of ~ 1000 RPM, the aligned fibers show alignment across ~ 50 μm length scales as reflected by a single peak in the orientation angle distribution across three replicates (Fig. 2Aii); by contrast, we observe multiple peaks across varying orientation angles for unaligned nanofibers (Fig. 2Aiv). Given that nanofiber diameter can also affect muscle cell alignment, growth, and myogenesis (Narayanan et al., 2020) and the diameter of nanofibers can differ with spinning conditions (Huttunen & Kellomäki, 2011), we confirm that there is no statistical difference between the diameter of aligned ($d = 200 \pm 36$ nm) and unaligned ($d = 215 \pm 36$ nm) nanofibers ($p = 0.06$) (Supplementary Fig. 2A). Since the mechanical properties of scaffolds across ~μm length scales of cells can also influence cellular behaviors (Wells, 2008; Xu et al., 2017), we confirm the stiffness of aligned and unaligned nanofiber scaffolds using AFM; this data reveal that both aligned and unaligned scaffolds have similar stiffness with a Young's modulus of 69 ± 29 kPa for aligned scaffolds and 60 ± 15 kPa for unaligned scaffolds ($p = 0.34$) (Supplementary Fig. 2B). While these scaffolds are stiffer than skeletal muscle that typically has a Young's modulus of 8 – 15 kPa (Lapin et al., 2013), aligned nanofibers can promote desired behaviors of myocytes, such as proliferation (Cooper et al., 2010) and differentiation into myotubes (Yeo & Kim, 2019).

3.2. Aligned nanofiber scaffolds promote alignment and myotube formation of rabbit and mouse myocytes

To compare the extent of myocyte differentiation on aligned versus unaligned nanofiber scaffolds, we test both myogenic primary rabbit (RbSkMC) and murine (C2C12) skeletal muscle cells. We induce differentiation by culturing cells with differentiation induction medium for 7 days. To quantify myotube alignment, we immunostain cells to visualize myosin heavy chain (Myh4) and measure the orientation of Myh4 positive myotubes using angle distribution analysis (Fig. 2B,C). Myotubes on aligned nanofiber scaffolds show alignment over ~ mm length scales, as indicated by the defined peak in the orientation distribution curves

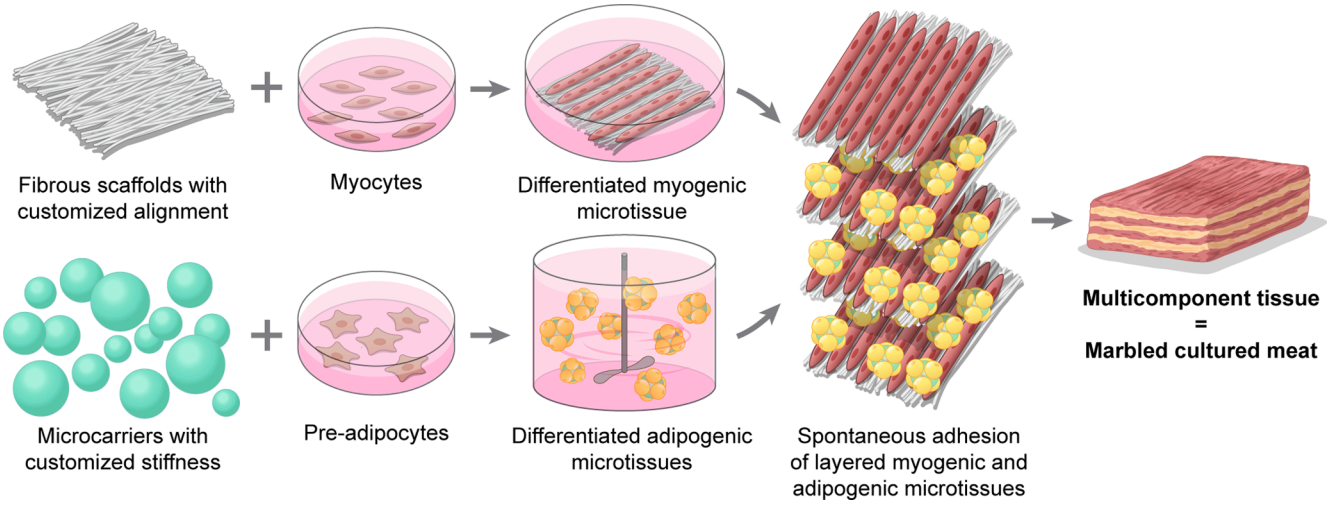

Fig. 1. Schematic of modular approach to generate marbled cultured meat. Precursor muscle cells (myocytes) are seeded on aligned fibrous scaffolds that are fabricated using electrospinning. Adipocyte precursors (pre-adipocytes) are seeded on microcarrier scaffolds generated using water-in-oil emulsions as templates. Cells are grown and differentiated in their respective media and bioreactors. After harvesting post-differentiation, myogenic and adipogenic microtissues are stacked and spontaneously adhere to form intact multicomponent tissue or marbled cultured meat.

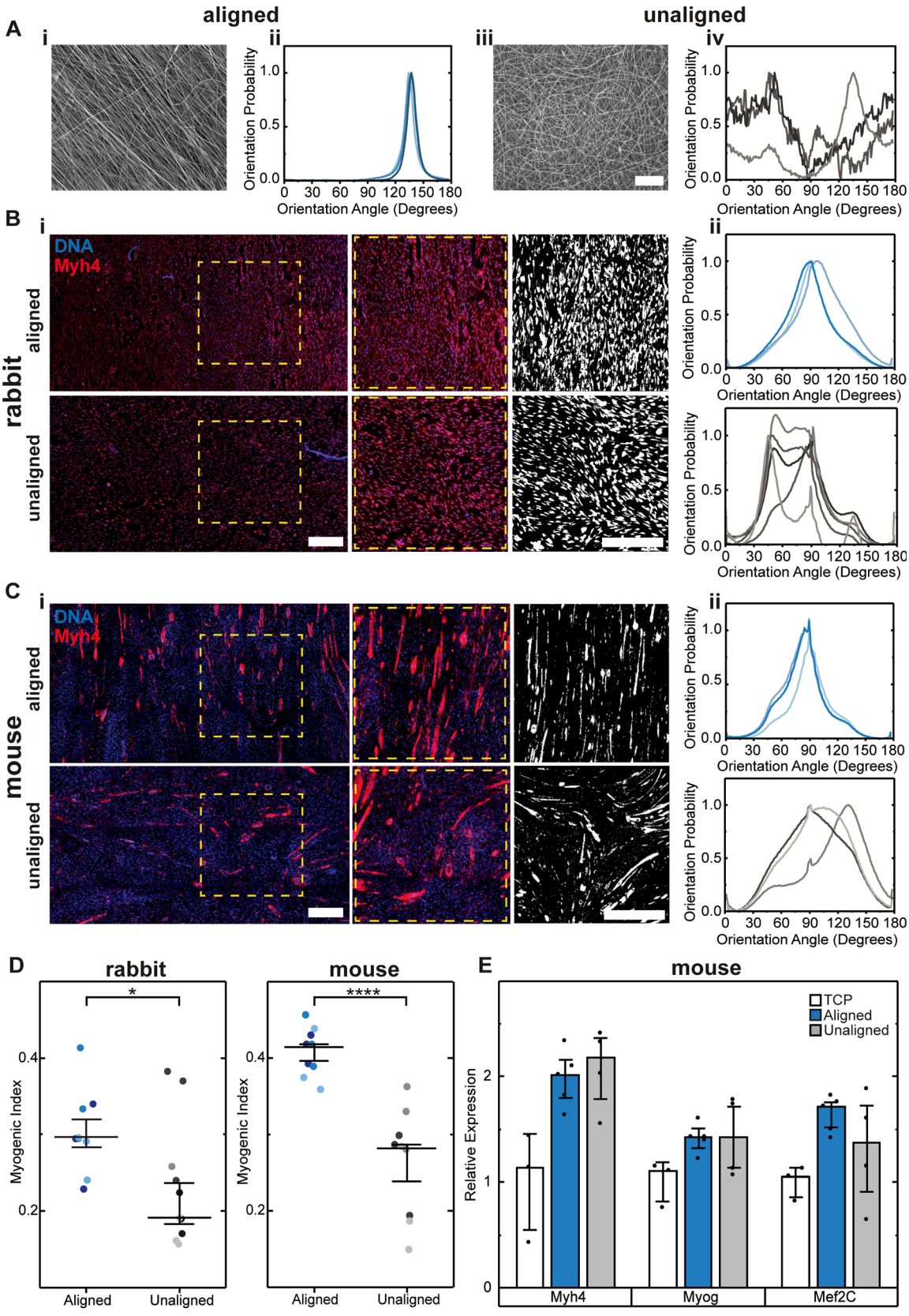

(caption on next page)

Fig. 2. Producing myogenic microtissues on nanofiber scaffolds. (**A**) Characterization of gelatin nanofiber scaffolds. Representative scanning electron microscopy images of dried gelatin (i) aligned and (iii) unaligned nanofibers. Scale, 10 μm. Orientation analysis of (ii) aligned and (iv) unaligned nanofibers from 3 independent experiments. Representative images of (**B**)(i) RbSkMC and (**C**)(i) C2C12 on aligned and unaligned gelatin nanofibers after culture with differentiation induction medium for 7 days. Dashed yellow boxes denote insets, which are displayed in the middle and right columns. The right column is the thresholded version of the image shown in the middle column. Scale, 500 μm. Distribution of orientation angles of myotubes immunolabeled with anti-myosin heavy chain (Myh4, red) signal of (**B**)(ii) RbSkMC and (**C**)(ii) C2C12 and on aligned versus unaligned nanofibers. (**D**) The myogenic index quantifies the number of nuclei identified by DNA (blue, Hoechst) localized within a myotube relative to the total number of nuclei in the field of view. Data for RbSkMC and C2C12 cells on aligned and unaligned scaffolds obtained across 3 independent experiments. Subreplicates measured within a single experiment are represented by a single color. Horizontal lines show median values; error bars represent the standard deviation. Statistical significance determined using a Mann Whitney *U* test, * $p < 0.05$, **** $p < 0.0001$. (**E**) Relative expression of myogenic differentiation markers Myh4, Myogenin, and Mef2C for C2C12 cells on tissue culture plastic (TCP), aligned and unaligned nanofiber scaffolds using qRT-PCR. Data across 3 independent experiments; a $p > 0.05$ determined by a Wilcoxon Rank-Sum test.

reflecting how the majority of fibers share a similar orientation. By contrast, the myotubes cultured on the unaligned scaffolds show a broader distribution of orientation angles, which is consistent with the random distribution of fibers across length scales of ~ 1 to 5 mm. While the myotube orientations in the unaligned scaffolds are generally isotropic, we observe some fiber alignment across smaller length scales of ~ 500 μm, as indicated by the multiple smaller peaks in the orientation distribution plots. We next assess the efficiency of differentiation for cells on aligned versus unaligned nanofibers by determining the myogenic index, or the number of nuclei in myotubes (cells containing 3 or more nuclei) divided by the total number of nuclei. Both rabbit and murine samples show an increased myogenic index for cells on aligned versus unaligned nanofiber scaffolds, consistent with the increased number of myotubes on aligned scaffolds (for rabbit $p = 0.01$; for mouse, $p < 0.0001$) (Fig. 2D). We further assess markers of myogenesis at the transcript level for murine cells on aligned versus unaligned nanofiber scaffolds by measuring the expression of Myh4, Myogenin, and Mef2C using qRT-PCR (Fig. 2E). While there is no significant difference in Myh4, Myogenin, or Mef2C transcript levels between cells on aligned and unaligned nanofiber scaffolds, all three myogenic markers exhibit a trend of higher expression on aligned nanofiber scaffolds as compared to tissue culture plastic.

3.3. Compliant microbeads support the growth of adipogenic microtissues

Since 3T3-L1 adipocytes show increased lipid accumulation on more compliant $E \sim 2$ kPa scaffolds compared to > 10 kPa scaffolds (Chandler et al., 2011), we generate compliant, $E \sim 4$ kPa, gelatin microbeads as scaffolds for adipose tissue culture using water-in-oil emulsions as a template. Using a size-filtration protocol that we previously developed (Norris et al., 2022), we produce microbeads with a total surface area per batch ranging from $\sim 2 \times 10^3$ to 1×10^5 μm^2, which is standard for microcarriers used for cell culture (Microcarrier Cell Culture: Principles and Methods. GE Healthcare Handbook., 2005) (Fig. 3A). We confirm the Young's modulus of the gelatin microbeads is 4.4 ± 0.51 kPa using AFM (Fig. 3A-ii).

To quantify adipogenesis for cells on microbead scaffolds, we culture primary rabbit pre-adipocytes from subcutaneous fat (RbPreAd) and murine pre-adipocytes (3T3-L1) on the microbeads in suspension culture. After 7 days of proliferation, cultures are subsequently differentiated for an additional 7 days with differentiation induction medium. Over the 14 day time course, we observe a trend towards accumulation of intracellular lipids in both rabbit and mouse adipocytes, as evidenced by the increased signal of LipidTox, which is a marker for neutral lipids (Fig. 3B). The 3T3-L1 adipocytes show a ~ 100 × increase in lipid area per cell over the 14 day timescale as revealed by quantitative image analysis (Fig. 3C). We find a similar trend of lipid accumulation in the rabbit RbPreAd cells—albeit with only a ~ 20 × increase. To further quantify adipogenesis at the transcript level, we measure levels of adipogenic markers (PPARγ, CEBPα) in 3T3-L1 cells using qRT-PCR. As shown in Fig. 3D, we find no statistical difference in the expression of PPARγ and CEBPα between cells grown on the two culture substrates, indicating that the microbeads support adipogenesis of 3T3-L1 cells as sufficiently as standard tissue culture plastic.

3.4. Modular and tunable approach to engineer 3D multicomponent tissue

Towards engineering marbled cultured meat, we use a modular approach to build 3D multicomponent tissue from myogenic and adipogenic microtissues. We generate myogenic microtissues by seeding myocytes on aligned electrospun nanofibers. In parallel, we produce adipogenic microtissues by culturing adipocytes on compliant microbeads. After growth and differentiation of each microtissue component in their respective differentiation media, we harvest and stack microtissues to generate a multicomponent tissue construct. As shown in Fig. 5, the proof-of-concept multicomponent tissue has three layers of myogenic microtissue and two layers of adipogenic microtissue.

Within ~ hours after stacking, we observe that microtissues adhere to each other to form a 3D multicomponent tissue construct. To gain insight into the spontaneous microtissue adhesion process, we mechanically perturb layered myogenic and adipogenic microtissues by rigorous nutation at 6 h intervals over an 18 h time course after stacking. Using quantitative image analysis, we assess how intact the microtissue stack remains after nutation by quantifying the projected surface area of microtissue that is displaced after the mechanical perturbation. Using this analysis, we estimate a relative adhesion index for microtissues over time post stacking. For murine myogenic and adipogenic microtissues generated on gelatin scaffolds, we find that stacked microtissues form an intact tissue within ~ 6 h post stacking as revealed by the increase in relative adhesion index over time (Fig. 4A). Microtissues generated with primary rabbit cells on plant-based scaffolds form an intact structure within ~ 6 h, as revealed by the increase in the relative adhesion index after the 0 h time point (Fig. 4Bi, iv). We also find that murine microtissues cultured with plant-based scaffolds show an increase in relative adhesion index over ~ 6 – 12 h timescales (Fig. 4Bii, v). By contrast, stacks of scaffolds without cells disperse after nutating 18 h post stacking (Fig. 4Biii, vi), indicating that cells are required to mediate the spontaneous adhesion of microtissues into an intact multicomponent tissue construct. Since scaffold mechanical properties could impact the adhesion process, we compare the stiffness of the plant-based scaffolds to the gelatin scaffolds. The Young's modulus of soy microbeads is 30 ± 9 kPa and zein microfiber scaffolds is 0.6 ± 0.4 kPa (Supplementary Fig. 5). By contrast, the Young's modulus of gelatin microbeads is 4.4 ± 0.51 kPa and gelatin nanofibers is between 60 ± 15 kPa (unaligned scaffolds) and 69 ± 29 kPa (aligned scaffolds). Thus, spontaneous adhesion occurs for microtissues cultured with scaffolds that have varying stiffness, suggesting that scaffold mechanics are not a major contributor to the adhesion process. Taken together, these results suggest that multicomponent tissue composed of different types of cells and scaffolds can be generated through the spontaneous adhesion of microtissues on ~ 6 – 12 h timescales.

To visualize the structure and spatial organization of the multicomponent myogenic-adipogenic tissue constructs, we immunostain and image samples generated with gelatin scaffolds using confocal microscopy (Fig. 5A-C). To image the myogenic component of the tissue, we use the muscle-specific marker Myh4; to image the adipogenic microtissue component we immunolabel PPARγ in the composite tissue. To further visualize the spatial organization of intracellular neutral lipids in

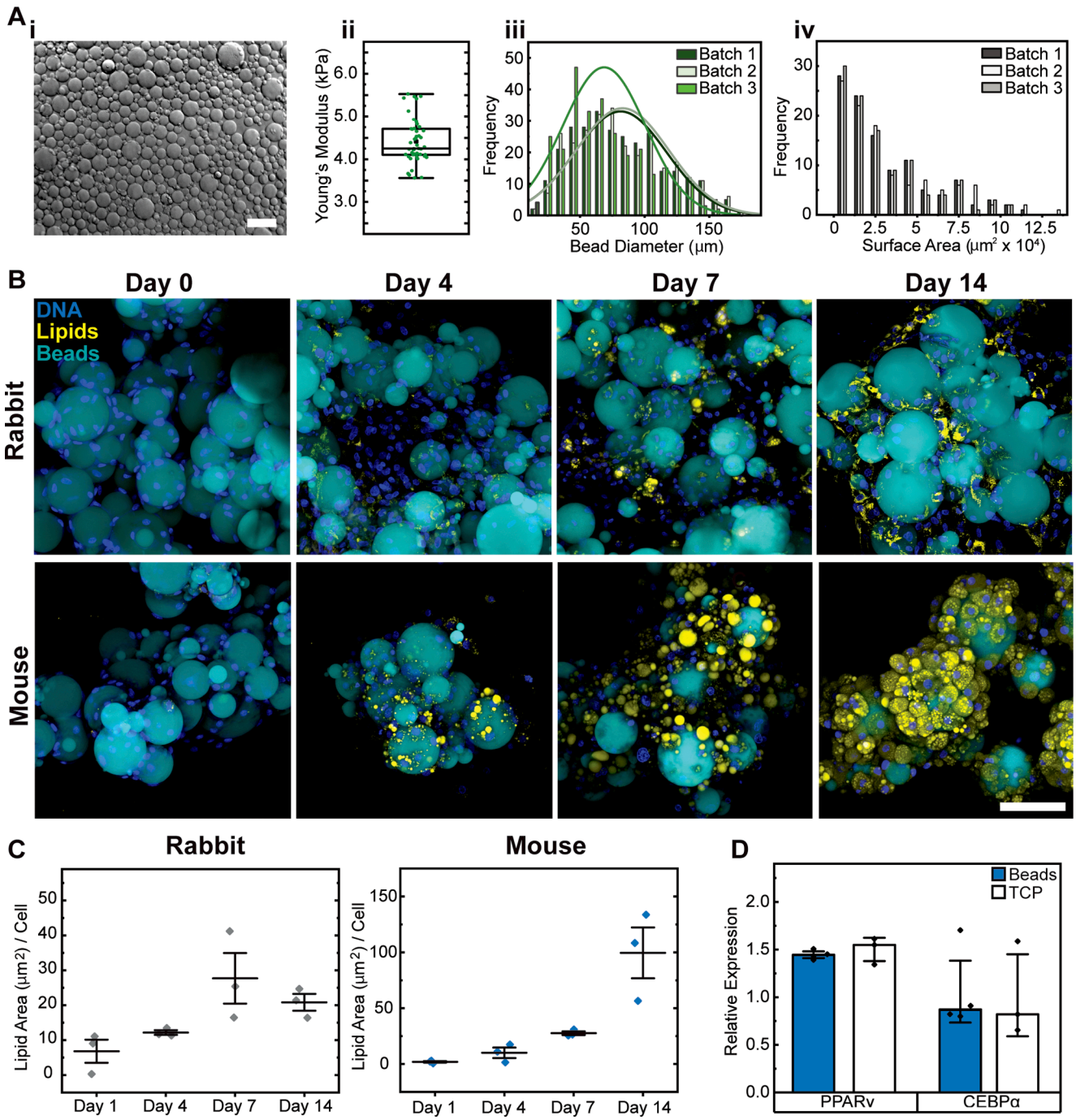

Fig. 3. Producing adipogenic microtissues in suspension culture. (**A**) Characterization of gelatin microbeads for adipose tissue culture. (i) Brightfield image of gelatin microbeads in 1 × PBS. Scale, 200 μm. (ii) Young's modulus of microbeads quantified using AFM (n = 47 beads across 2 independent experiments). (iii) Diameter (μm) and (iv) surface area ($\mu m^2 \times 10^4$) distribution of microbeads in 1 × PBS (n = 1200 beads across 3 independent experiments). (**B**) Primary rabbit subcutaneous adipocytes (top) and 3T3-L1 murine adipocytes (bottom) are cultured on microbeads in suspension culture and imaged at 0, 4, 7, and 14 days of differentiation. Images show DNA (blue, Hoechst), intracellular lipids (yellow, LipidTox) and gelatin microbeads (cyan). Images of individual components are shown in Supplementary Fig. 3. Scale, 100 μm. (**C**) Intracellular lipid area per cell measured using quantitative image analysis for RbPreAd and 3T3-L1 cells. To determine the average lipid area per cell, we divide the total lipid area by the total number of nuclei, which is quantified using Hoechst. Horizontal lines show median values; error bars represent the standard deviation. $p > 0.05$ determined by a Wilcoxon Rank-Sum test. (**D**) Relative expression of adipogenic markers, Peroxisome proliferator-activated receptor gamma (PPARγ) and CCAAT/enhancer-binding protein alpha (CEBPα), in differentiated 3T3-L1 cells on microbeads (n = 4) versus tissue culture plastic (TCP, n = 3) after 7 days of differentiation using qRT-PCR. Bars show median values; error bars represent the standard deviation. $p > 0.05$ determined by a Wilcoxon Rank-Sum test.

the myogenic-adipogenic tissue construct—which are prominent in the adipose component of the tissue—we use LipidTox and Nile Red. Three-dimensional reconstructions generated from confocal images reveal that Myh4-positive cells are integrated within the adipogenic microtissue layer; these findings indicate that the myogenic and adipogenic microtissues are in close proximity to each other and appear to be well integrated 18 h after stacking (Fig. 5B).

To further assess the spatial organization of the myogenic-adipogenic

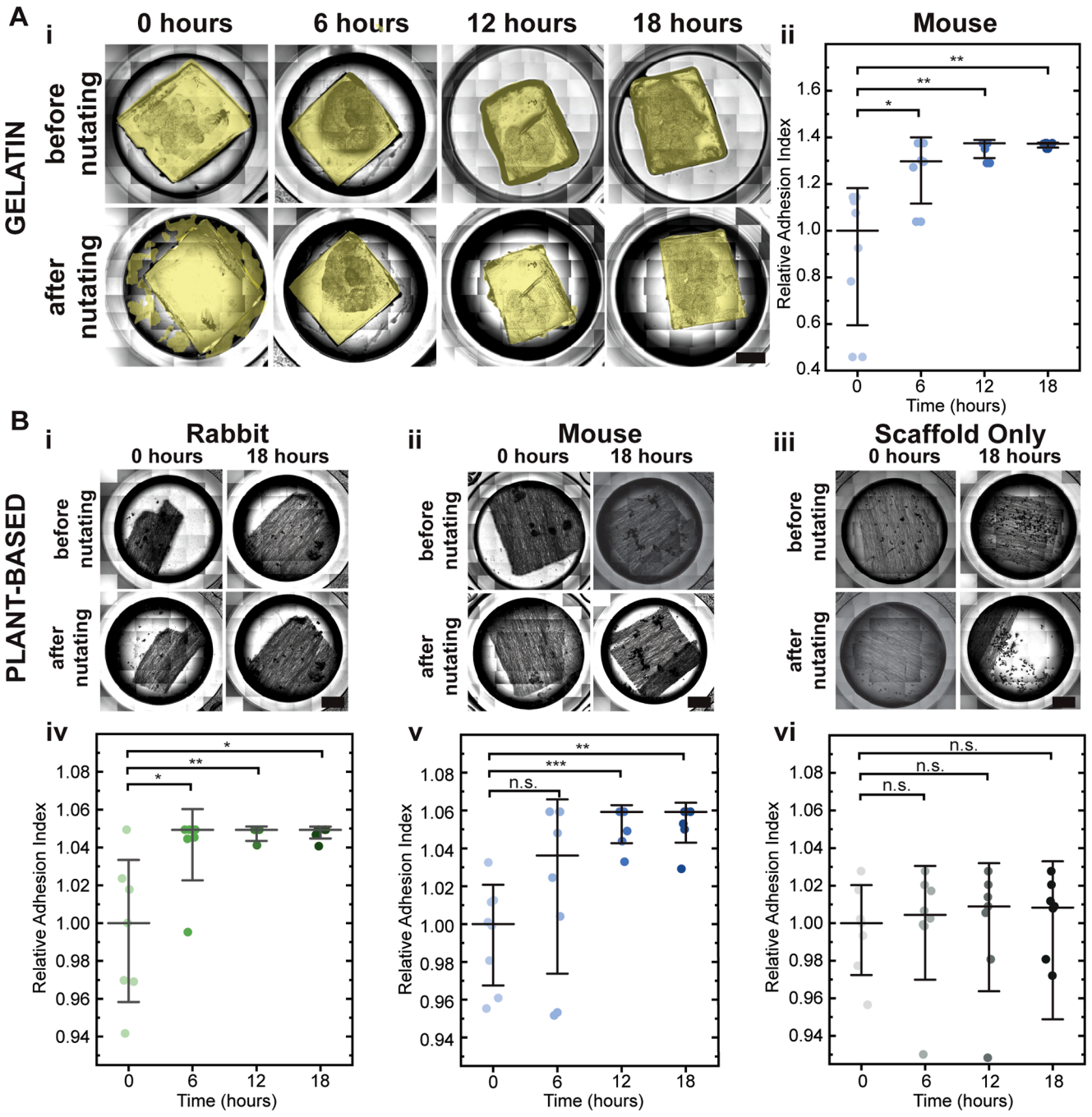

Fig. 4. Spontaneous adhesion of myogenic and adipogenic microtissues to form intact 3D multicomponent tissue constructs. (**A**) Microtissues cultured with gelatin scaffolds: (i) Brightfield images of differentiated C2C12 skeletal muscle cells on gelatin nanofibers layered with differentiated 3T3-L1 adipocytes on gelatin microbeads before and after 2 min of rigorous nutation at 100 RPM in 1 × PBS at 0, 6, 12, and 18 h timepoints post stacking. Images are tiled to provide a view of the entire well of the culture dish. Yellow overlay shows projected surface area. Scale, 2 mm. (ii) Relative adhesion index data for mouse myogenic and adipogenic microtissues cultured with gelatin scaffolds. The relative adhesion index is quantified by evaluating the projected surface area (SA) of the microtissue/scaffold stack before and after nutating, $[100 - (SA_{before} - SA_{after})]$. Values are normalized to the median relative adhesion index at time zero for each dataset. Horizontal lines show median values; error bars represent the standard deviation. Statistical significance determined using a Mann Whitney *U* test, *p < 0.05, **p < 0.01. (**B**) Microtissues cultured with plant-based scaffolds: Tiled brightfield images of differentiated primary (i) rabbit skeletal muscle cells on zein microfiber scaffolds layered with differentiated primary rabbit adipocytes on soy microcarriers, (ii) differentiated C2C12 skeletal muscle cells on zein microfiber scaffolds layered with differentiated 3T3-L1 adipocytes on soy microcarriers, and (iii) zein microfiber scaffolds layered with soy microcarriers without cells before and after nutating in 1 × PBS at 0 and 18 h timepoints post stacking. Scale, 2 mm. Relative adhesion index of (iv) rabbit myogenic and adipogenic microtissues with plant-based scaffolds, (v) mouse myogenic and adipogenic microtissues with plant-based scaffolds, and (vi) plant-based scaffolds only. Horizontal lines show median values; error bars represent the standard deviation. Statistical significance determined using a Mann Whitney *U* test, *p < 0.05, **p < 0.01. ***p < 0.001, n.s. = not significant, p > 0.05.

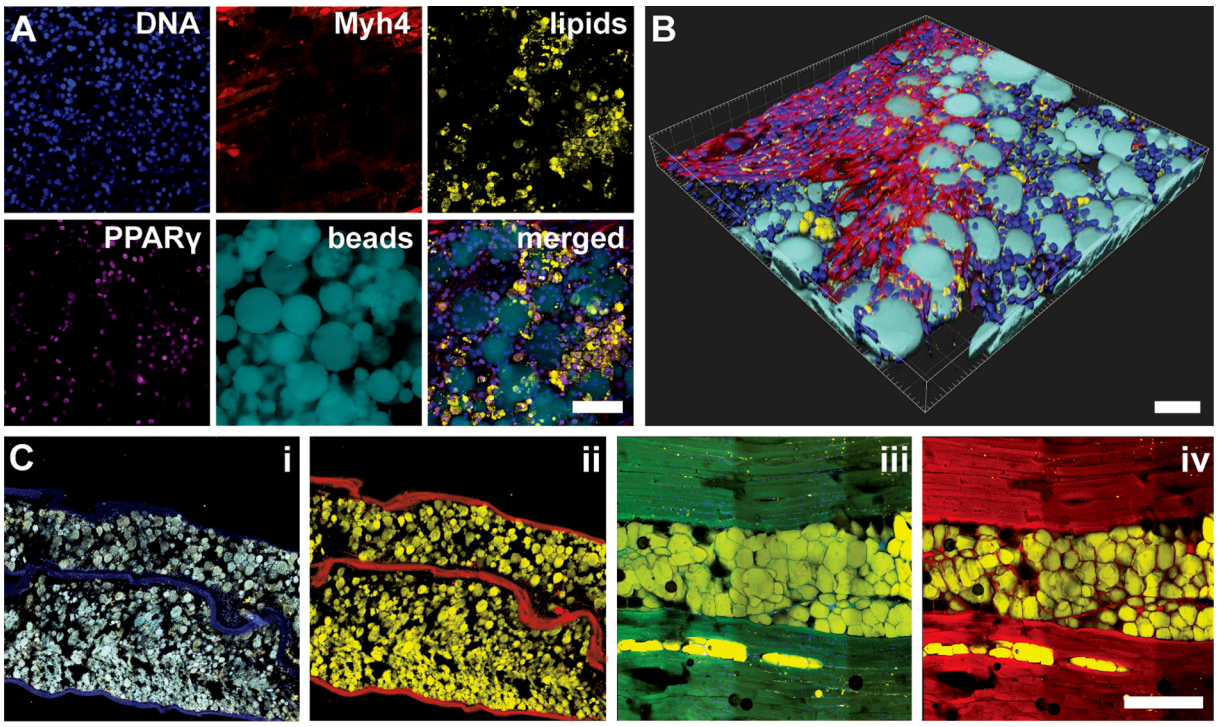

Fig. 5. Multicomponent myogenic-adipogenic tissue constructs. (**A**) Differentiated C2C12 skeletal muscle cells on aligned gelatin nanofibers layered with differentiated 3T3-L1 adipocytes on gelatin microbeads. DNA (blue, Hoechst), Myh4 (red), intracellular lipids (yellow, LipidTox), PPARγ (purple), and microbeads (cyan). Scale, 100 μm. (**B**) Composite tissue construct composed of rabbit myogenic and adipose microtissues. Reconstructed 3D images generated from stacks of confocal images of differentiated skeletal muscle cells on aligned gelatin nanofibers layered with differentiated adipocytes on gelatin microbeads. All images of direct-from-culture MT samples are acquired using confocal microscopy after 18 h post stacking. DNA (blue, Hoechst), Myh4 (red), intracellular lipids (yellow, LipidTox), and beads (cyan). Scale, 100 μm. (**C**) Cryosectioned (i) rabbit multicomponent tissue stained for DNA (blue, Hoechst), intracellular lipids (yellow, Nile Red), and microbeads (cyan). (iii) Wagyu steak stained for DNA (blue, Hoechst), intracellular lipids (yellow, Nile Red), and protein (green, FITC). False-colored images of (ii) rabbit multicomponent tissue and (iv) Wagyu beef steak samples to visualize the organization and structure of myogenic (red) and adipogenic (yellow) microtissue layers. Scale, 500 μm.

tissue construct, we generate cross-sections of the tissue by cryosectioning, staining, and imaging via confocal microscopy (Fig. 5Ci). Images of tissue cross-sections reveal stacked layers of myogenic and adipogenic microtissue. Within the myogenic component, myotubes are proximal to the nanofibers of the electrospun scaffold, which span the ~ 50 – 100 μm thickness of each myogenic tissue layer. The microbeads and adipocytes are prominent within the interspersed layers of adipogenic microtissue, spanning the ~ 200 μm – 1 mm thickness of each adipogenic microtissue layer. Based on quantitative image analysis of this proof-of-concept multicomponent tissue, we estimate the ratio of myogenic cells to adipogenic cells by volume to range from ~ 1 – 1.5 for both rabbit and mouse samples. We also estimate the total cell density in the multicomponent tissues to range from 4 to 8 $\times 10^8$ cells/cm^3 for both mouse and rabbit samples (Supplementary Fig. 6).

To compare the spatial structure of the engineered marbled cultured meat to conventionally produced meat, we image cryosections of a Wagyu beef steak as a commercially-relevant structural homolog that exhibits marbling (Fig. 5Ciii). The Wagyu steak shows intramuscular fat features that have a length scale ranging from 100 μm to 1 mm in thickness, which is consistent with previous reports in the literature (Valenzuela et al., 2020). While the length scale of the myogenic microtissue in the multicomponent cultured meat is only ~ 50 – 100 μm compared to the ~ mm muscle component of the conventional Wagyu steak, the ~ 1 mm length scale of the adipogenic tissue layers in the marbled cultured meat is comparable to the intramuscular fat of the Wagyu steak.

3.5. Multicomponent tissue exhibits properties of a viscoelastic solid material

We next characterize the mechanical properties of the myogenic-adipogenic tissue constructs using a parallel plate rheometer. If the myogenic and adipogenic microtissues are adhered together into a cohesive piece of marbled cultured meat, the tissue will exhibit properties of a solid that resists deformation. By contrast if the individual tissue components are not fully adhered to each other, the microtissue layers would slip and the composite tissue would break apart into the individual myogenic and adipogenic microtissue components. To assess the resistance of the multicomponent tissue to varying magnitudes of applied strain, we place the harvested myogenic-adipogenic tissue construct produced with gelatin scaffolds between the plates of a parallel plate rheometer (Fig. 6). We first evaluate direct-from-culture multicomponent tissue that is placed in the rheometer immediately after harvesting from culture. We find that the myogenic-adipogenic tissue resists increasing magnitudes of applied strain elastically up to a yield strain of $\gamma_y \approx 0.1$, indicating the sample exhibits properties of a solid material. In conjunction, we find that the small-strain plateau shear elastic modulus, G'_p, ranges from 0.1 kPa to 0.2 kPa. We also observe a minor degree of dissipative loss through the loss modulus $G''/G'_p \approx 0.1$ (*i.e.* the loss tangent) in the linear-response regime; such loss has been previously observed in the mechanical behavior of viscoelastic biological materials, including many foods (Singh et al., 2006). We next compare the mechanical properties of the multicomponent tissue with a conventionally produced Wagyu steak. The Wagyu sample shows an increased G'_p of 5 to 6 kPa and resistance to applied strain up to $\gamma_y =$ 0.01 to 0.02. Since the G'_p value of the Wagyu is significantly higher than the multicomponent tissue, we next determine the effects of post-harvest

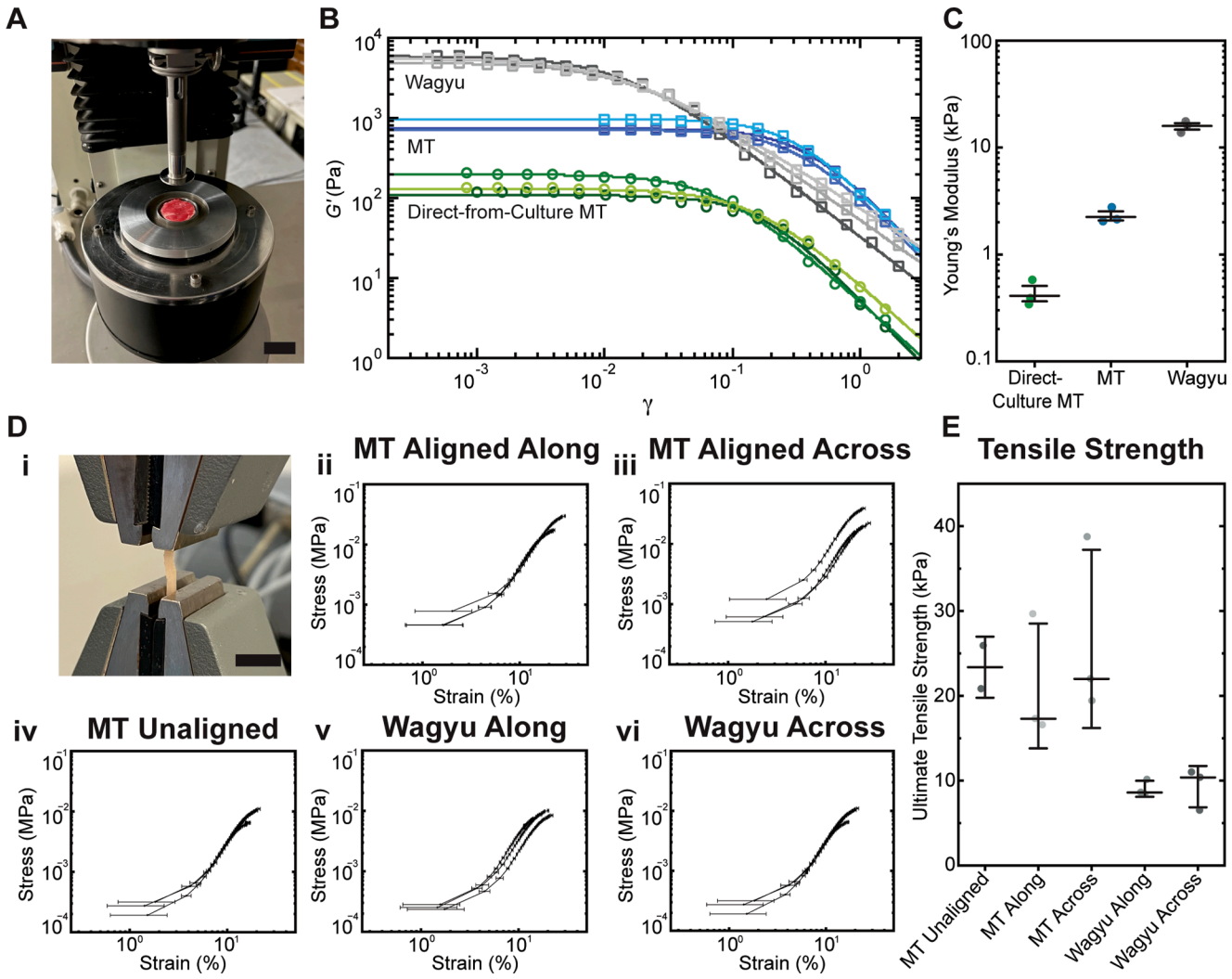

Fig. 6. Mechanical characterization of multicomponenttissue (MT) constructs that contain layered murine myogenic and adipogenic microtissues. (**A**) A parallel plate rheometer is used to quantify the mechanical properties of MT constructs and Wagyu beef steak. Shown here is a thin slice of Wagyu steak in the rheometer. (**B**) Data showing G' measured across a strain sweep measured at RT. Prior to measurement MT samples are placed on filter paper for 24 h at 4 °C after harvesting from the culture medium. The direct-from-culture MT sample is measured immediately after harvesting from culture medium. The Wagyu steak is a ~ 1 mm thick slice of conventionally produced marbled Wagyu beef steak. Three individual datasets are represented with different shades of colors and with different colors for each type of sample. For all samples, the high-strain power law exponent kappa lies in the range of 1.0 to 1.7 (Supplementary Table 1). (**C**) Young's modulus values determined from G'_p. Horizontal lines represent average of three independent samples; error bars show standard deviation. $p > 0.05$ determined by a Wilcoxon Rank-Sum test. (**D**) A force measurement system is used to quantify the tensile properties of MT constructs and Wagyu beef steak. All tensile analysis is performed on MT samples that are placed on filter paper for 24 h at 4 °C after harvesting. (i) Shown here is a strip of multicomponent tissue loaded in the instrument. Stress/strain curves of (ii) myogenic-adipogenic MT where the myogenic tissue is cultured with aligned nanofiber scaffolds and the tensile stress is applied in the same direction as the fiber alignment; (iii) myogenic-adipogenic MT where the myogenic tissue is cultured with aligned nanofiber scaffolds and the tensile stress is applied orthogonally to the fiber alignment; (iv) myogenic-adipogenic MT where the myogenic tissue is cultured with unaligned nanofiber scaffolds; (v) conventionally produced Wagyu steak where the tensile stress is applied along the direction of the muscle fibers; and (vi) conventionally produced Wagyu steak where the tensile stress is applied orthogonally to the muscle fibers. Three individual datasets are represented with separate tensile curves. (**E**) The ultimate tensile strength of each sample is quantified by measuring the maximum stress at which the sample breaks. Horizontal lines show median values; error bars represent the standard deviation. $p > 0.05$ determined by a Wilcoxon Rank-Sum test.

processing. Inspired by the post-slaughter processing of beef through aging (Ijaz et al., 2020), we test if we could achieve cultured multicomponent tissue with higher G'_p values that are more similar to the Wagyu by placing the multicomponent tissue on filter paper for 24 h prior to the rheological measurements. We observe that after 24 h on filter paper post-harvest, multicomponent tissue samples exhibit a higher resistance to increasing magnitudes of applied strain up to $\gamma_y =$ 0.32 to 0.37, and a higher G'_p ranging from 0.7 kPa to 1 kPa (Fig. 6B). It is important to note that while we find a parallel plate analysis to be most appropriate for flat tissue samples, the strain yield is not uniform across the plate and thus represents an average across the tissue. These initial findings indicate the potential of tuning the post-harvest processing to modulate the texture of marbled cultured meat.

To compare the mechanical properties of multicomponent tissues to conventional meat, we estimate the Young's modulus of marbled cultured meat and Wagyu steak using G'_p (Fig. 6C). Assuming a Poisson's ratio of 0.5 as quantified for gelatin (van Otterloo & Cruden, 2016), we find the Young's modulus of murine myogenic-adipogenic tissue is 2 to 3 kPa. For comparison, we measure the Young's modulus of a Wagyu steak to range from ~ 14 to 18 kPa assuming a Poisson's ratio of 0.45 as determined for bovine skeletal muscle (Kim et al., 2013). By contrast, the Young's modulus of the direct-from-culture multicomponent tissue is 0.3 to 0.6 kPa. These findings are consistent with the scaling of the Young's modulus of protein network with polymer density (Panteli &

Patrickios, 2018) given the expected decrease in water content during the 24 h post-harvest period on filter paper.

We next determine the tensile properties of the multicomponent tissue, including whether scaffold alignment affects the bulk mechanical properties of the tissue. Interestingly we observe a similar median tensile strength of 17 – 23 kPa across both unaligned and aligned samples regardless of the direction if the tensile stress is applied either in the same direction or orthogonally to the nanofiber alignment (Fig. 6). We speculate this may be due to the additional chemical crosslinking of nanofiber scaffolds before seeding cells, which impacts mechanical stability both within and between nanofibers in the myogenic microtissue. These findings may also reflect that the mechanical stability of multicomponent tissue is dominated by cell–cell and cell-matrix interactions. To compare the tensile properties of the marbled cultured meat to conventional meat, we conduct similar analysis of Wagyu beef steak samples, either applying tensile stress along the direction of muscle fibers or orthogonally to the grain. We also do not observe any significant difference in the stress/strain response of Wagyu steak when pulled along or against the grain; these results are consistent with a previous findings (Lepetit & Culioli, 1994). Our findings reveal that the ultimate tensile strength of multicomponent tissue regardless of the fiber orientation is $\sim 23 \pm 7$ kPa and $\sim 9 \pm 2$ kPa for the Wagyu steak; however, these differences are not statistically significant (Fig. 6).

We next assess MT properties that are important for cultured meat as a food product, including the protein content and cooking loss. Since meat is an important source of dietary protein and an essential macronutrient (Willett et al., 2019), protein content will be an important feature of cultured meat products. We quantify protein content in both raw rabbit and murine multicomponent tissues using a BCA Protein Assay Kit. As shown in Fig. 7A, protein content for both rabbit and murine samples is $\sim 4 \pm 2$ g/ 100 g. While the protein content of murine and mouse MT is lower than the protein content measured in Wagyu steaks ($\sim 9 \pm 4$ g/ 100 g), there is also variability across samples and no statistical difference between the protein content of rabbit MT versus Wagyu steak ($p = 0.11$) (Fig. 7A). It is important to note that these values are relative to the total sample mass and therefore sensitive to water content, which may be lower in the Wagyu samples, given that the majority of beef cuts are typically aged for $\sim$ 21 days post-slaughter (Ramanathan et al., 2020).

An important determinant of cookability and meat quality—including juiciness—is the cooking loss (Aaslyng et al., 2003), which estimates the loss of aqueous and lipid components in a sample during the cooking process. To assess cooking loss of the marbled cultured meat, we cook the cultured meat samples in a clamshell grill. We find that the marbled cultured meat exhibits signs of browning (Fig. 7Bi), which is characteristic of Maillard reactions (Ellis, 1959). Both rabbit and mouse marbled cultured meat samples show a median cooking loss of $\sim$ 30 %, which is higher although not statistically different than the $\sim$ 20 % cooking loss observed for the Wagyu steak samples (Fig. 7Bii). Interestingly, gelatin-only control samples show a trend towards increased cooking loss and less browning (Supplementary Fig. 7), suggesting that the cellular component of MT may be important for MT properties during cooking.

4. Discussion

To produce marbled cultured meat with desired palatability, scalable strategies to integrate engineered adipose tissue into cultured meat will be critical. Here we show a modular approach to generate marbled cultured meat with both myogenic and adipogenic components that spontaneously adhere to form stable tissue constructs with $\sim$ mm- to cm-scale dimensions. The key innovation in our approach is the engineering of scaffolds with customized physical properties that provide the foundation for the spontaneous adhesion of myogenic and adipogenic cells and microtissues into multicomponent 3D tissue constructs without the use of additional crosslinkers.

4.1. Modular approach to build multicomponent tissues through spontaneous adhesion enables customization of growth conditions for different cell types

Using a modular approach to engineer marbled cultured meat enables myocytes and adipocytes to be cultured separately using optimized media and scaffold conditions; the resultant myogenic and adipogenic microtissues can then be harvested and assembled into a multicomponent 3D tissue constructs that has properties of a viscoelastic solid material. We find that the adhesion of microtissues into an intact tissue construct occurs on timescales of $\sim 6 – 12$ h across murine cell lines and primary rabbit cells on both gelatin and plant-derived scaffolds. Our findings reveal that cells are required for microtissue adhesion, suggesting that the spontaneous adhesion process may be facilitated by cell–cell and/or cell-scaffold interactions.

While it can be feasible to co-culture different cell types in an open bioreactor (Ben-Arye et al., 2020), the use of media and scaffolds that are customized for individual cell types has potential to accelerate desired cell phenotypes (Beldjilali-Labro et al., 2018; Choi et al., 2010; Guex et al., 2012; Syverud, VanDusen, & Larkin, 2016; Yuen et al., 2023), and ultimately increase the efficiency of cultured meat production. For example, the optimal differentiation of myocytes requires low serum conditions (Ricotti et al., 2012) while adipocytes require high serum conditions (Zebisch et al., 2012); these contrasting media formulations are a limitation for simultaneously culturing myogenic and adipogenic components of cultured meat in an open bioreactor system. The methodology we present here builds on previous approaches to customize the physical properties of scaffolds for skeletal muscle tissue engineering (Choi et al., 2008; Engler et al., 2004; MacQueen et al., 2019). Importantly, we establish the use of scaffolds with customized physical properties for engineering adipose tissue, which we anticipate

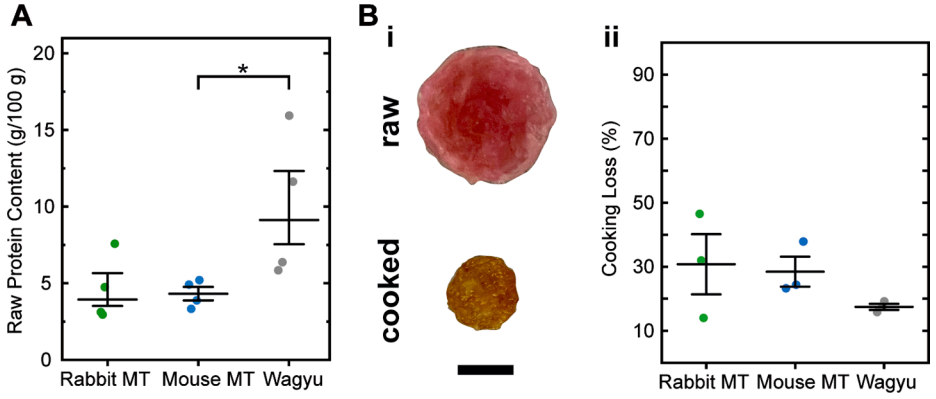

Fig. 7. Protein content and cooking loss of multicomponent tissue. (**A**) Protein content (g/100 g) of raw multicomponent tissue (Rabbit multicomponent tissue (MT), Mouse MT) versus conventional Wagyu beef steak. Horizontal lines show median values; error bars represent the standard deviation. Data is analyzed using a Wilcoxon Rank-Sum test, * $p < 0.05$; n.s. = not significant, $p > 0.05$. (**B**) (i) Representative images of rabbit MT before and after cooking. Scale, 1 cm. (ii) Cooking loss of rabbit MT, mouse MT, and Wagyu beef steak determined by the mass of sample cooked to an internal temperature of 65 °C versus raw sample. Horizontal lines show median values; error bars represent the standard deviation. Data is analyzed using a Wilcoxon Rank-Sum test, $p > 0.05$.

will be an important contributor to achieving cultured meat that will be desired by consumers (Yuen et al., 2023). The modular approach we describe to build multicomponent tissue has the potential to complement existing approaches such as cell sheets (Shahin-Shamsabadi & Selvaganapathy, 2021), hydrogel molds (Zagury et al., 2022), and 3D printed cell-scaffold constructs (Kang et al., 2021; Li et al., 2022; Zagury et al., 2022). While 3D printing can be used to deposit individual muscle and fat tissue components within a multicomponent tissue, mechanical stabilization is achieved by the addition of crosslinkers such as transglutaminase (Kang et al., 2021) or calcium chloride (Zagury et al., 2022). Here, we find that the spontaneous adhesion of myogenic and adipogenic microtissues results in the formation of a mechanically stable multicomponent tissue that does not require additional crosslinkers or reagents, and thus has potential to increase process efficiency, especially when brought to scale. Future work will investigate the molecular mechanisms underlying the spontaneous adhesion process, which relies on cell-matrix and cell–cell adhesions and we hypothesize is thus mediated by integrins, cadherins, and/or dystroglycan (Bachmann et al., 2019; Moore & Winder, 2010; Sheikh et al., 2022), and can have broader implications for the layer-by-layer assembly of tissues.

4.2. Potential to circumvent diffusion limitations using the modular approach to engineer 3D tissue constructs

By relying on the spontaneous adhesion of microtissues to form intact macroscale 3D tissue constructs, the modular approach we present here also has potential to overcome diffusion limitations that challenge the production of >100 μm – 1 mm thick tissue in the absence of vasculature (Rouwkema et al., 2008). We separately culture myogenic microtissues that are 30 to 50 μm in thickness and adipogenic microtissues that range from 100 to 500 μm in diameter; both the myogenic and adipogenic microtissues remain within the size range that allows for the exchange of nutrients and metabolites on timescales of $\sim$ hours (McMurtrey, 2016); further, culturing microtissues in a bioreactor with mixing or perfusion may further promote nutrient and metabolite exchange. Once the microtissues are stacked, they form a cohesive multicomponent myogenic-adipogenic tissue construct over $\sim 6 - 12$ h, which eliminates the need for prolonged co-culture. To enable the transport of oxygen and nutrients over longer timescales, the modular scaffold approach could be easily adapted to increase exchange of oxygen and nutrients, for example by fabricating scaffolds with higher porosity (Ianovici et al., 2022; Zaszczyńska et al., 2021). Other strategies to enhance mass transport between layers within a tissue construct could include integrating a third endothelial cell component into the modular multicomponent tissue (Ben-Arye et al., 2020; Kang et al., 2021).

4.3. Potential to optimize efficiency of cultured meat production using customized scaffolds

Here we demonstrate how the modular approach to produce multicomponent tissue constructs is compatible with scaffolds that are customized for myogenic and adipogenic cells. We culture myogenic microtissues using aligned nanofiber scaffolds, which mimic the native structure of skeletal muscle (Schiaffino & Reggiani, 2011). We observe increased alignment and formation of myotubes for both rabbit and mouse microtissues grown on aligned nanofibers versus unaligned nanofibers which is consistent with previous findings (Huang et al., 2006). However, we do not find any significant differences in transcript levels of myogenic differentiation markers in mouse C2C12 myotubes. Our observations are consistent with previous findings showing that despite increased myotube formation there are no significant differences in mRNA expression of myogenic markers in skeletal muscle cells grown on unaligned versus aligned scaffolds (Chen et al., 2015), but contrast other reports that scaffold alignment increases myogenic markers at the transcript level in skeletal muscle cells (Yeo et al., 2016); these conflicting results can likely be attributed to differences in scaffold design and culture conditions. Future work will be needed to determine the relationship between the expression of myogenic markers such as Myh4, Myog, and Mef2C and the texture and sensory properties of cultured meat. We speculate that the physical structure of the microtissue—which is determined by the scaffolds and alignment of myotubes—may be a stronger determinant of cultured meat texture and sensory properties than gene expression patterns alone. Scaffold topology and stiffness could also be tuned to accelerate the growth of microtissues for cultured meat. Cell proliferation is regulated by matrix stiffness (Wells, 2008), and murine muscle stem cells show increased expansion on a polyethylene glycol hydrogel with elastic modulus, $E \sim 12$ kPa, compared to stiffer, polystyrene petri dishes (Gilbert et al., 2010). The physical properties of scaffolds could also be designed to enhance the overall texture of cultured meat. For example, engineering myogenic tissue comprised of aligned myotubes and/or scaffolds with aligned topologies may contribute to the 'grain' or anisotropic mechanical properties of steak (Bailey, 1972). While our findings here reveal similar tensile properties across multicomponent tissue generated with aligned versus unaligned nanofiber scaffolds, the nanofiber scaffolds we use here are crosslinked after electrospinning, which results in mechanical stabilization within and between fibers. We observe similar tensile properties of Wagyu steak when samples are stretched along or orthogonally to the direction of the muscle fibers. It is plausible that cultured meat generated with nanofiber scaffolds that have reduced crosslinking may better replicate the tensile properties of Wagyu steak. Future work will examine how the physical properties of scaffolds on the micron-scale impact the mechanical properties, texture, and mouthfeel of marbled cultured meat on the macroscale.

To support the growth of adipogenic microtissue, we culture adipogenic cells using microbeads with $E \sim 4$ kPa; mouse 3T3-L1 adipocytes cultured within hydrogel scaffolds of similar stiffness show increased lipid accumulation compared to cells grown on stiffer scaffolds (Chandler et al., 2011). We observe similar levels of adipogenic differentiation markers in mouse adipocytes grown on the compliant $\sim$ 4 kPa microbeads compared to tissue culture plastic, which has $\sim 1 \times 10^4$ MPa stiffness but also has different surface properties than the gelatin microbeads. The behavior of cells may also differ on the 2D substrate provided by the tissue culture plastic versus within the 3D microtissues, which are aggregates of cells and microbeads. In addition, cells in 2D are cultured in static conditions whereas the 3D microtissues experience suspension culture conditions that may include fluid shear stresses and increased mass transport. Future studies will decipher the effects of microbead stiffness on adipose microtissue growth. In addition, it will be valuable to determine the effects of microbead stiffness on adipogenesis; the accumulation of lipids in adipocytes is a desired phenotype as fatty acids within lipid droplets can affect the flavor and nutritional profile of cultured meat (Elmore et al., 1999).

4.4. Towards a scalable approach

While the proof-of-concept marbled cultured meat that we present here is engineered on the laboratory scale, our approach has potential for scale-up. Nanofiber scaffolds are fabricated using electrospinning, an approach that is currently being used in pharmaceutical (Omer et al., 2021) and textile (Persano et al., 2013) industries, although we recognize there may be unique challenges in scaling up electrospinning for food applications. The hydrogel microbead scaffolds are templated using water-in-oil emulsions, which are widely used in the food industry and can be generated on industrial scales (Degner et al., 2014; McClements, 2010). Microbead scaffolds can also support the culture of cells in a suspension bioreactor (Liu et al., 2022; Norris et al., 2022), which will be important to facilitate the scale-up required to produce $\sim$ kgs of cultured meat for food consumption. Harnessing the ability of microtissues to adhere into intact 3D tissue constructs further has potential for scale-up: the generation of multicomponent tissue relies on the spontaneous adhesion of myogenic and adipogenic microtissues that is

mediated by cells and does not require additional crosslinkers. While we demonstrate here a manual approach to generating multicomponent tissue constructs, automated methods for stacking microtissues will need to be developed to achieve scaled-up production.

Here we show the potential value of scaffolds to seed the growth of microtissues, which are spontaneously adhering building blocks for multicomponent tissues, but the use of scaffolds requires additional raw materials, fabrication processes, and sterilization. Yet there are potential additional advantages of utilizing scaffolds to support the growth of cultured meat. Scaffolds can contribute to the volume of cultured meat and thus reduce the number of cells required for the final product. Furthermore, scaffolds can provide topographical and mechanical stimuli that could accelerate microtissue growth, promote the growth of tissues that mimics the structure and texture of natural muscle, and ultimately contribute to the final sensory and nutritional properties of cultured meat. A comprehensive mapping of the costs and benefits of scaffolds for cultured meat production at scale will require technoeconomic assessments as well as life cycle analyses.

It is important to note that the proof-of-concept data showing feasibility of the layer-by-layer assembly of multicomponent tissues uses scaffolds composed of gelatin, zein, and soy. To generate the customized scaffolds, we use gelatin, which is a commonly added ingredient to enhance mouthfeel of meat products (Baziwane & He, 2003) and a natural ECM-derived component that enables mammalian cell attachment without further need for functionalization. The electrospinning and emulsion-based methods we use to produce customized scaffolds can be readily adapted to other edible polymers including but not limited to microbially-derived gelatin (Báez et al., 2005), agarose (Nyberg et al., 2017), alginate (Ianovici et al., 2022; Tahir & Floreani, 2022), wheat glutenin (Xiang, Yuen Jr, et al., 2022), and zein (Xiang, Yao, et al., 2022). We show the spontaneous adhesion approach to generating multicomponent tissue is translatable to microtissues cultured on zein and soy scaffolds; plant-based scaffolds are desired to reduce dependence on livestock agriculture. The modular approach we present should further be compatible with other types of plant-based scaffolds, for example, that use food industry byproducts such as textured soy protein (Ben-Arye et al., 2020). However, additional chemical processing to functionalize plant-based polymers may be required to promote animal cell adhesion, which could add complexity and cost to processing. Adapting the approach for future food applications will also require testing with serum-free media (Stout et al., 2022) (Mitić et al., 2023), which will be critical to address the scalability challenge. In this proof-of-concept study we use standard cell culture procedures including fetal bovine serum; the spontaneous adhesion process for generating marbled cultured meat may depend on cell, scaffold, and media combinations.

4.5. Envisioning delicious marbled cultured meat

A central goal in the field is to mimic the native structure of marbled meat. Here, we generate cultured meat that has adipose microtissue features on the ~ 200 μm-1 mm length scale, which is similar to length scales of intramuscular fat in conventional Wagyu beef steak (Fig. 5C). Mimicking the length scales of myogenic tissue features in our marbled cultured meat will require further optimization to tune the dimensions and ratios of myogenic and adipogenic components. In addition, our observations show that marbled cultured meat—even when derived from rabbit and mouse cells—exhibits protein content and cooking loss that is similar to conventional Wagyu beef. Future work will determine the extent to which scaffolds contribute to the protein content of the marbled cultured meat. Identifying how scaffolding materials affect the taste, mouthfeel, and nutritional content of marbled cultured meat will also be a valuable direction of future studies.

The mechanical properties of the proof-of-concept marbled cultured meat that we present here show some similarities to the conventional Wagyu beef steak, but there are also clear differences. The multicomponent tissue constructs generated from mouse cells show resistance to shear stress, reflecting that the multicomponent tissue has solid-like properties similar to conventional beef steak. Importantly, we show that the post-culture processing has marked impacts on the mechanical properties of the multicomponent tissue. By placing the multicomponent tissue on filter paper for 24 h, we achieve an order of magnitude increase in the Young's modulus of the tissue construct. While the Young's modulus of multicomponent tissue is still an order of magnitude lower than the Wagyu steak, we envision that the post-harvest processing steps could be tuned to achieve desired texture of marbled cultured meat. For example, the harvested tissue construct could be chilled and stored until consumption—or 'aged'—akin to processing steps of meat following animal slaughter (Ijaz et al., 2020). We hypothesize that further aging could reduce the water content of the tissue, result in less cooking loss, and thereby improve the cookability of cultured meat. However, simply focusing on generating cultured meat with an increased Young's modulus may result in a more rubbery-like texture (Sinha & Bhargav, 2020). Therefore, it may be important to also consider engineering cultured meat with a reduced yield strain to give a more tender mouthfeel similar to a Wagyu steak. The tensile properties are also important for meat: higher amounts of connective tissue are associated with increased tensile strengths and inversely correlated with meat tenderness (Stanley et al., 1972). We find that the tensile strengths of multicomponent tissue samples are slightly higher but not statistically different than Wagyu beef steak. Further texture profile analysis and sensory panels will be needed to assess the texture and mouthfeel of cultured meat that are relevant for palatability. Finally, while a major thrust of research focuses on engineered mimics of steak, there is also exciting potential to engineer novel cultured foods that surpass the texture, flavor, and nutritional profiles of conventional products.

5. Conclusion

In summary, we present here a modular approach to build multicomponent tissue using myogenic and adipogenic microtissues as building blocks. The spontaneous adhesion of microtissues to form multicomponent tissue constructs should have exciting potential for scale-up. Utilizing a modular strategy provides the ability to customize the scaffold physical properties and culture environment for individual cell types with potential to circumvent diffusion limitations when engineering multicomponent tissue. Our proof-of-concept findings show the approach can be used to build 3D multicomponent tissue with ~ mm to ~ cm scale dimensions through the self-adhesion of myogenic and adipogenic tissue layers. Ultimately the structured integration of adipose tissue into cultured muscle tissues will be critical to engineer delicious cultured meat products from marbled steaks to salmon filets and beyond.

Funding

This work was supported by the United States Department of Agriculture National Institute of Food and Agriculture, AFRI project CALW-2021-09608; the New Harvest Foundation (Fellowship to NSK and Seed Grant to AD); the Good Food Institute; the National Science Foundation Innovations at the Nexus of Food, Energy, and Water Systems (INFEWS) training grant (DGE-1735325, which supported NSK & KC); a National Science Foundation Boosting Research Ideas for Transformative and Equitable Advances in Engineering (BRITE) Fellow Award (to ACR); and the UCLA California NanoSystems Institute and the Noble Family Innovation Fund; and the State of California. SCPN was supported by the National Institute of Dental & Craniofacial Research of the National Institutes of Health under Award Number F32DE030004.

Declaration of Competing Interest

The authors declare that they have no known competing financial interests or personal relationships that could have appeared to influence the work reported in this paper.

Data availability

Data will be made available on request.

Acknowledgements

The authors would like to thank Wesley Kawecki for his assistance in fabricating the custom-built rotating aluminum collection cylinder used to electrospin nanofibers, Dr. Eric Deeds for his expert advice on statistical analysis, and Yu-Ting L. Dingle, Ph.D., of Pipette & Stylus LLC, for her assistance with illustrations. The authors acknowledge the use of instruments at the Nano & Pico Characterization Lab at the California NanoSystems Institute and the MCDB/BSCRC Microscopy Core.

Appendix A. Supplementary material

Supplementary data to this article can be found online at https://doi.org/10.1016/j.foodres.2023.113080.

References

Aaslyng, M. D., Bejerholm, C., Ertbjerg, P., Bertram, H. C., & Andersen, H. J. (2003). Cooking loss and juiciness of pork in relation to raw meat quality and cooking procedure. *Food Quality and Preference, 14*(4), 277–288.

Allan, S. J., De Bank, P. A., & Ellis, M. J. (2019). Bioprocess design considerations for cultured meat production with a focus on the expansion bioreactor. *Frontiers in Sustainable Food Systems, 3*, 44.

Bachmann, M., Kukkurainen, S., Hytönen, V. P., & Wehrle-Haller, B. (2019). Cell adhesion by integrins. *Physiological Reviews, 99*(4), 1655–1699.

Báez, J., Olsen, D., & Polarek, J. W. (2005). Recombinant microbial systems for the production of human collagen and gelatin. *Applied Microbiology and Biotechnology, 69*(3), 245–252.

Bailey, A. J. (1972). The basis of meat texture. *Journal of the Science of Food and Agriculture, 23*(8), 995–1007.

Baziwane, D., & He, Q. (2003). Gelatin: The paramount food additive. *Food Reviews International, 19*(4), 423–435.

Beldjilali-Labro, M., Garcia Garcia, A., Farhat, F., Bedoui, F., Grosset, J.-F., Dufresne, M., & Legallais, C. (2018). Biomaterials in tendon and skeletal muscle tissue engineering: Current trends and challenges. *Materials, 11*(7), 1116.

Ben-Arye, T., Shandalov, Y., Ben-Shaul, S., Landau, S., Zagury, Y., Ianovici, I., … Levenberg, S. (2020). Textured soy protein scaffolds enable the generation of three-dimensional bovine skeletal muscle tissue for cell-based meat. *Nature Food, 1*(4), 210–220.

Chandler, E. M., Berglund, C. M., Lee, J. S., Polacheck, W. J., Gleghorn, J. P., Kirby, B. J., & Fischbach, C. (2011). Stiffness of photocrosslinked RGD-alginate gels regulates adipose progenitor cell behavior. *Biotechnology and Bioengineering, 108*(7), 1683–1692.

Chen, A.-K.-L., Chen, X., Choo, A. B. H., Reuveny, S., & Oh, S. K. W. (2011). Critical microcarrier properties affecting the expansion of undifferentiated human embryonic stem cells. *Stem Cell Research, 7*(2), 97–111.

Chen, S., Nakamoto, T., Kawazoe, N., & Chen, G. (2015). Engineering multi-layered skeletal muscle tissue by using 3D microgrooved collagen scaffolds. *Biomaterials, 73*, 23–31.

Choi, J. H., Gimble, J. M., Lee, K., Marra, K. G., Rubin, J. P., Yoo, J. J., … Kaplan, D. L. (2010). Adipose tissue engineering for soft tissue regeneration. *Tissue Engineering Part B: Reviews, 16*(4), 413–426.

Choi, J. S., Lee, S. J., Christ, G. J., Atala, A., & Yoo, J. J. (2008). The influence of electrospun aligned poly (epsilon-caprolactone)/collagen nanofiber meshes on the formation of self-aligned skeletal muscle myotubes. *Biomaterials, 29*(19), 2899–2906.

Churchill, W. S. (2016). *Thoughts and adventures*. Rosetta Books.

Comley, K., & Fleck, N. A. (2010). A micromechanical model for the Young's modulus of adipose tissue. *International Journal of Solids and Structures, 47*(21), 2982–2990.

Cooper, A., Jana, S., Bhattarai, N., & Zhang, M. (2010). Aligned chitosan-based nanofibers for enhanced myogenesis. *Journal of Materials Chemistry, 20*(40), 8904–8911.

Degner, B. M., Chung, C., Schlegel, V., Hutkins, R., & McClements, D. J. (2014). Factors influencing the freeze-thaw stability of emulsion-based foods. *Comprehensive Reviews in Food Science and Food Safety, 13*(2), 98–113.

Ellis, G. (1959). The maillard reaction. In *Advances in Carbohydrate Chemistry* (Vol. 14, pp. 63–134). Elsevier.

Elmore, J. S., Mottram, D. S., Enser, M., & Wood, J. D. (1999). Effect of the polyunsaturated fatty acid composition of beef muscle on the profile of aroma volatiles. *Journal of Agricultural and Food Chemistry, 47*(4), 1619–1625.

Engler, A. J., Griffin, M. A., Sen, S., Bönnemann, C. G., Sweeney, H. L., & Discher, D. E. (2004). Myotubes differentiate optimally on substrates with tissue-like stiffness pathological implications for soft or stiff microenvironments. *Journal of Cell Biology, 166*(6), 877–887.

Fischbach, C., Seufert, J., Staiger, H., Hacker, M., Neubauer, M., Göpferich, A., & Blunk, T. (2004). Three-dimensional in vitro model of adipogenesis: Comparison of culture conditions. *Tissue Engineering, 10*(1–2), 215–229.

Fountain, H. (2013). A Lab-Grown Burger Gets a Taste Test. *The New York Times*. https://www.nytimes.com/2013/08/06/science/a-lab-grown-burger-gets-a-taste-test.html.

Frye, C. A., & Patrick, C. W. (2006). Three-dimensional adipose tissue model using low shear bioreactors. *In Vitro Cellular & Developmental Biology-Animal, 42*(5–6), 109–114.

Furuhashi, M., Morimoto, Y., Shima, A., Nakamura, F., Ishikawa, H., & Takeuchi, S. (2021). Formation of contractile 3D bovine muscle tissue for construction of millimetre-thick cultured steak. *NPJ Science of Food, 5*(1), 1–8.

Gherman, E. D., & Bălan, I. M. (2022). Bioengineered Meat and it's Potential Contributions to Food Security in the Future-A Literature Review. *Scientific Papers: Animal Science & Biotechnologies/Lucrari Stiintifice: Zootehnie si Biotehnologii, 55*(1).

Gilbert, P. M., Havenstrite, K. L., Magnusson, K. E., Sacco, A., Leonardi, N. A., Kraft, P., … Blau, H. M. (2010). Substrate elasticity regulates skeletal muscle stem cell self-renewal in culture. *Science, 329*(5995), 1078–1081.

Guex, A., Kocher, F., Fortunato, G., Körner, E., Hegemann, D., Carrel, T., … Giraud, M.-N. (2012). Fine-tuning of substrate architecture and surface chemistry promotes muscle tissue development. *Acta Biomaterialia, 8*(4), 1481–1489.

Hocquette, J.-F., Gondret, F., Baéza, E., Médale, F., Jurie, C., & Pethick, D. (2010). Intramuscular fat content in meat-producing animals: Development, genetic and nutritional control, and identification of putative markers. *Animal, 4*(2), 303–319.

Huang, N. F., Patel, S., Thakar, R. G., Wu, J., Hsiao, B. S., Chu, B., … Li, S. (2006). Myotube assembly on nanofibrous and micropatterned polymers. *Nano Letters, 6*(3), 537–542.

Huttunen, M., & Kellomäki, M. (2011). A simple and high production rate manufacturing method for submicron polymer fibres. *Journal of Tissue Engineering and Regenerative Medicine, 5*(8), e239–e243.

Ianovici, I., Zagury, Y., Redenski, I., Lavon, N., & Levenberg, S. (2022). 3D-printable plant protein-enriched scaffolds for cultivated meat development. *Biomaterials, 284*, Article 121487.

Ijaz, M., Jaspal, M. H., Hayat, Z., Yar, M. K., Badar, I. H., Ullah, S., … Farooq, M. Z. (2020). Effect of animal age, postmortem chilling rate, and aging time on meat quality attributes of water buffalo and humped cattle bulls. *Animal Science Journal, 91*(1), e13354.

Kang, D.-H., Louis, F., Liu, H., Shimoda, H., Nishiyama, Y., Nozawa, H., … Nagamori, E. (2021). Engineered whole cut meat-like tissue by the assembly of cell fibers using tendon-gel integrated bioprinting. *Nature Communications, 12*(1), 1–12.

Kim, H., Yoo, L., Shin, A., & Demer, J. L. (2013). Determination of poisson ratio of bovine extraocular muscle by computed X-ray tomography. *BioMed Research International, 2013*, 197479.

Kim, M. S., Lee, B., Kim, H. N., Bang, S., Yang, H. S., Kang, S. M., … Jeon, N. L. (2017). 3D tissue formation by stacking detachable cell sheets formed on nanofiber mesh. *Biofabrication, 9*(1), Article 015029.

Kumar, A., Accorsi, A., Rhee, Y., & Girgenrath, M. (2015). Do's and don'ts in the preparation of muscle cryosections for histological analysis. *JoVE (Journal of Visualized Experiments), 99*, e52793.

Lapin, M., Gonzalez, J., & Johnson, S. (2013). Substrate elasticity affects bovine satellite cell activation kinetics in vitro. *Journal of Animal Science, 91*(5), 2083–2090.

Leal-Calderon, F., Thivilliers, F., & Schmitt, V. (2007). Structured emulsions. *Current Opinion in Colloid & Interface Science, 12*(4–5), 206–212.

Lepetit, J., & Culioli, J. (1994). Mechanical properties of meat. *Meat Science, 36*(1–2), 203–237.

Li, C.-H., Yang, I.-H., Ke, C.-J., Chi, C.-Y., Matahum, J., Kuan, C.-Y., … Lin, F.-H. (2022). The production of fat-containing cultured meat by stacking aligned muscle layers and adipose layers formed from gelatin-soymilk scaffold. *Frontiers in Bioengineering and Biotechnology, 10*.

Liu, Y., Wang, R., Ding, S., Deng, L., Zhang, Y., Li, J., … Yan, X. (2022). Engineered meatballs via scalable skeletal muscle cell expansion and modular micro-tissue assembly using porous gelatin micro-carriers. *Biomaterials, 121615*.

MacQueen, L. A., Alver, C. G., Chantre, C. O., Ahn, S., Cera, L., Gonzalez, G. M., … Motta, S. E. (2019). Muscle tissue engineering in fibrous gelatin: Implications for meat analogs. *NPJ Science of Food, 3*(1), 1–12.

McClements, D. J. (2010). Emulsion design to improve the delivery of functional lipophilic components. *Annual Review of Food Science and Technology, 1*(1), 241–269.

McMurtrey, R. J. (2016). Analytic models of oxygen and nutrient diffusion, metabolism dynamics, and architecture optimization in three-dimensional tissue constructs with applications and insights in cerebral organoids. *Tissue Engineering Part C: Methods, 22*(3), 221–249.

Microcarrier Cell Culture: Principles and Methods. GE Healthcare Handbook. (2005). (Vol. No. 18-1140-62).

Mitić, R., Cantoni, F., Börlin, C. S., Post, M. J., & Jackisch, L. (2023). A simplified and defined serum-free medium for cultivating fat across species. *Iscience, 26*(1), Article 105822.

Moore, C. J., & Winder, S. J. (2010). Dystroglycan versatility in cell adhesion: A tale of multiple motifs. *Cell Communication and Signaling, 8*, 1–12.

Mott, P., & Roland, C. (2009). Limits to Poisson's ratio in isotropic materials. *Physical Review B, 80*(13), Article 132104.
Narayanan, N., Jiang, C., Wang, C., Uzunalli, G., Whittern, N., Chen, D., … Deng, M. (2020). Harnessing fiber diameter-dependent effects of myoblasts toward biomimetic scaffold-based skeletal muscle regeneration. *Frontiers in Bioengineering and Biotechnology, 8*, 203.
Nishimura, T., Hattori, A., & Takahashi, K. (1999). Structural changes in intramuscular connective tissue during the fattening of Japanese black cattle: Effect of marbling on beef tenderization. *Journal of Animal Science, 77*(1), 93–104.
Noidad, S., Limsupavanich, R., Suwonsichon, S., & Chaosap, C. (2019). Effect of visual marbling levels in pork loins on meat quality and Thai consumer acceptance and purchase intent. *Asian-Australasian Journal of Animal Sciences, 32*(12), 1923.
Norris, S. C., Kawecki, N. S., Davis, A. R., Chen, K. K., & Rowat, A. C. (2022). Emulsion-templated microparticles with tunable stiffness and topology: Applications as edible microcarriers for cultured meat. *Biomaterials, 121669*.
Nyberg, K. D., Hu, K. H., Kleinman, S. H., Khismatullin, D. B., Butte, M. J., & Rowat, A. C. (2017). Quantitative deformability cytometry: Rapid, calibrated measurements of cell mechanical properties. *Biophysical Journal, 113*(7), 1574–1584.
O'Quinn, T. G., Legako, J. F., Brooks, J., & Miller, M. F. (2018). Evaluation of the contribution of tenderness, juiciness, and flavor to the overall consumer beef eating experience. *Translational Animal Science, 2*(1), 26–36.
Omer, S., Forgách, L., Zelkó, R., & Sebe, I. (2021). Scale-up of electrospinning: Market overview of products and devices for pharmaceutical and biomedical purposes. *Pharmaceutics, 13*(2), 286.
Panteli, P. A., & Patrickios, C. S. (2018). Complex hydrogels based on multiply interpenetrated polymer networks: Enhancement of mechanical properties via network multiplicity and monomer concentration. *Macromolecules, 51*(19), 7533–7545.
Persano, L., Camposeo, A., Tekmen, C., & Pisignano, D. (2013). Industrial upscaling of electrospinning and applications of polymer nanofibers: a review. *Macromolecular Materials and Engineering, 298*(5), 504–520.
Poncelet, D., Lencki, R., Beaulieu, C., Halle, J., Neufeld, R., & Fournier, A. (1992). Production of alginate beads by emulsification/internal gelation. I. Methodology. *Applied Microbiology and Biotechnology, 38*(1), 39–45.
Post, M. J., Levenberg, S., Kaplan, D. L., Genovese, N., Fu, J., Bryant, C. J., … Moutsatsou, P. (2020). Scientific, sustainability and regulatory challenges of cultured meat. *Nature Food, 1*(7), 403–415.
Qazi, T. H., Mooney, D. J., Pumberger, M., Geissler, S., & Duda, G. N. (2015). Biomaterials based strategies for skeletal muscle tissue engineering: Existing technologies and future trends. *Biomaterials, 53*, 502–521.
Ramanathan, R., Mafi, G., Yoder, L., Perry, M., Pfeiffer, M., VanOverbeke, D., & Maheswarappa, N. B. (2020). Biochemical changes of postmortem meat during the aging process and strategies to improve the meat quality. In *Meat Quality Analysis* (pp. 67–80). Elsevier.
Ricotti, L., Polini, A., Genchi, G. G., Ciofani, G., Iandolo, D., Vazao, H., … Pisignano, D. (2012). Proliferation and skeletal myotube formation capability of C2C12 and H9c2 cells on isotropic and anisotropic electrospun nanofibrous PHB scaffolds. *Biomedical Materials, 7*(3), Article 035010.
Rouwkema, J., Rivron, N. C., & van Blitterswijk, C. A. (2008). Vascularization in tissue engineering. *Trends in Biotechnology, 26*(8), 434–441.
Savell, J., Branson, R., Cross, H., Stiffler, D., Wise, J., Griffin, D., & Smith, G. (1987). National consumer retail beef study: Palatability evaluations of beef loin steaks that differed in marbling. *Journal of Food Science, 52*(3), 517–519.
Schiaffino, S., & Reggiani, C. (2011). Fiber types in mammalian skeletal muscles. *Physiological Reviews, 91*(4), 1447–1531.
Shahin-Shamsabadi, A., & Selvaganapathy, P. R. (2021). Engineering Murine Adipocytes and Skeletal Muscle Cells in Meat-like Constructs Using Self-Assembled Layer-by-Layer Biofabrication: A Platform for Development of Cultivated Meat. *Cells Tissues Organs*, 1–9.
Sheikh, M. O., Capicciotti, C. J., Liu, L., Praissman, J., Ding, D., Mead, D. G., … Moremen, K. W. (2022). Cell surface glycan engineering reveals that matriglycan alone can recapitulate dystroglycan binding and function. *Nature Communications, 13*(1), 3617.
Singh, A. P., Lakes, R. S., & Gunasekaran, S. (2006). Viscoelastic characterization of selected foods over an extended frequency range. *Rheologica Acta, 46*(1), 131–142.
Sinha, A., & Bhargav, A. (2020). Effect of state transition, drying kinetics and moisture content on Young's modulus variation during thermal drying of hygroscopic food materials. *Journal of Food Engineering, 279*, Article 109957.
Stanley, D., McKnight, L., Hines, W., Usborne, W., & Deman, J. (1972). Predicting meat tenderness from muscle tensile properties. *Journal of Texture Studies, 3*(1), 51–68.
Stout, A. J., Mirliani, A. B., Rittenberg, M. L., Shub, M., White, E. C., Yuen, J. S., & Kaplan, D. L. (2022). Simple and effective serum-free medium for sustained expansion of bovine satellite cells for cell cultured meat. *Communications Biology, 5*(1), 1–13.
Syverud, B. C., VanDusen, K. W., & Larkin, L. M. (2016). Growth factors for skeletal muscle tissue engineering. *Cells Tissues Organs, 202*(3–4), 169–179.
Tahir, I., & Floreani, R. (2022). Dual-Crosslinked Alginate-Based Hydrogels with Tunable Mechanical Properties for Cultured Meat. *Foods, 11*(18), 2829.
Tomiyama, A. J., Kawecki, N. S., Rosenfeld, D. L., Jay, J. A., Rajagopal, D., & Rowat, A. C. (2020). Bridging the gap between the science of cultured meat and public perceptions. *Trends in Food Science & Technology, 104*, 144–152.
Tuma, H., Henrickson, R., Stephens, D., & Moore, R. (1962). Influence of Marbling and Animal Age on Factors Associated with Beef Quality 1, 2, 3, 4. *Journal of Animal Science, 21*(4), 848–851.
Valenzuela, J., Lloyd, S., Mastaglia, F., & Dawkins, R. (2020). Adipose invasion of muscle in Wagyu cattle: Monitoring by histology and melting temperature. *Meat Science, 163*, Article 108063.
van Otterloo, J., & Cruden, A. R. (2016). Rheology of pig skin gelatine: Defining the elastic domain and its thermal and mechanical properties for geological analogue experiment applications. *Tectonophysics, 683*, 86–97.
Wells, R. G. (2008). The role of matrix stiffness in regulating cell behavior. *Hepatology, 47*(4), 1394–1400.
Willett, W., Rockström, J., Loken, B., Springmann, M., Lang, T., Vermeulen, S., … Wood, A. (2019). Food in the Anthropocene: The EAT–Lancet Commission on healthy diets from sustainable food systems. *The Lancet, 393*(10170), 447–492.
Wood, J., Enser, M., Fisher, A., Nute, G., Richardson, R., & Sheard, P. (1999). Manipulating meat quality and composition. *Proceedings of the Nutrition Society, 58*(2), 363–370.
Xiang, N., Yao, Y., Yuen, J. S., Jr, Stout, A. J., Fennelly, C., Sylvia, R., … Kaplan, D. L. (2022). Edible films for cultivated meat production. *Biomaterials, 287*, Article 121659.
Xiang, N., Yuen, J. S., Jr, Stout, A. J., Rubio, N. R., Chen, Y., & Kaplan, D. L. (2022). 3D porous scaffolds from wheat glutenin for cultured meat applications. *Biomaterials, 285*, Article 121543.
Xu, J., Sun, M., Tan, Y., Wang, H., Wang, H., Li, P., … Li, Y. (2017). Effect of matrix stiffness on the proliferation and differentiation of umbilical cord mesenchymal stem cells. *Differentiation, 96*, 30–39.
Yeo, M., & Kim, G. (2019). Nano/microscale topographically designed alginate/PCL scaffolds for inducing myoblast alignment and myogenic differentiation. *Carbohydrate Polymers, 223*, Article 115041.
Yeo, M., Lee, H., & Kim, G. H. (2016). Combining a micro/nano-hierarchical scaffold with cell-printing of myoblasts induces cell alignment and differentiation favorable to skeletal muscle tissue regeneration. *Biofabrication, 8*(3), Article 035021.
Yuen, J. S. K., Jr., Saad, M. K., Xiang, N., Barrick, B. M., DiCindio, H., Li, C., … Leung, G. (2023). Aggregating in vitro-grown adipocytes to produce macroscale cell-cultured fat tissue with tunable lipid compositions for food applications. *Elife, 12*, e82120.
Zagury, Y., Ianovici, I., Landau, S., Lavon, N., & Levenberg, S. (2022). Engineered marble-like bovine fat tissue for cultured meat. *Communications Biology, 5*(1), 1–12.
Zaszczyńska, A., Moczulska-Heljak, M., Gradys, A., & Sajkiewicz, P. (2021). Advances in 3D printing for tissue engineering. *Materials, 14*(12), 3149.
Zebisch, K., Voigt, V., Wabitsch, M., & Brandsch, M. (2012). Protocol for effective differentiation of 3T3-L1 cells to adipocytes. *Analytical Biochemistry, 425*(1), 88–90.